Article

Current Biology

Auxin boosts energy generation pathways to fuel pollen maturation in barley

Highlights

- Barley pollen autonomously produces high auxin levels to control its maturation
- The cereal-specific enzyme HvYUCCA4 synthesizes bioactive auxin in barley pollen
- Auxin is required to enhance the expression of central carbon metabolism genes
- Increased flux of energy production pathways fuels pollen starch accumulation

Authors

Dhika Amanda, Felix P. Frey, Ulla Neumann, ..., Alisdair R. Fernie, Karin Ljung, Iván F. Acosta

Correspondence

acosta@mpipz.mpg.de

In brief

As cereal pollen grains reach maturity, they form large starch deposits that later nourish them on their way to fertilization. Amanda et al. show that barley pollen produces the hormone auxin to control starch accumulation by enhancing central carbon metabolism pathways that generate energy as ATP, a limiting factor in the synthesis of starch.

Amanda et al., 2022, Current Biology *32*, 1–14
April 25, 2022
https://doi.org/10.1016/j.cub.2022.02.073

CellPress

Please cite this article in press as: Amanda et al., Auxin boosts energy generation pathways to fuel pollen maturation in barley, Current Biology (2022), https://doi.org/10.1016/j.cub.2022.02.073

Current Biology

CellPress

Article

Auxin boosts energy generation pathways to fuel pollen maturation in barley

Dhika Amanda,[1] Felix P. Frey,[1] Ulla Neumann,[1] Marine Przybyl,[1] Jan Šimura,[2] Youjun Zhang,[3,4] Zongliang Chen,[5] Andrea Gallavotti,[5,6] Alisdair R. Fernie,[3,4] Karin Ljung,[2] and Iván F. Acosta[1,7,*]

[1]Max Planck Institute for Plant Breeding Research, 50829 Cologne, Germany
[2]Umeå Plant Science Centre, Department of Forest Genetics and Plant Physiology, Swedish University of Agricultural Sciences, 90183 Umeå, Sweden
[3]Max Planck Institute of Molecular Plant Physiology, 14476 Potsdam, Germany
[4]Center of Plant Systems Biology and Biotechnology, 4000 Plovdiv, Bulgaria
[5]Waksman Institute of Microbiology, Rutgers University, Piscataway, NJ 08854, USA
[6]Department of Plant Biology, Rutgers University, New Brunswick, NJ 08901, USA
[7]Lead contact
*Correspondence: acosta@mpipz.mpg.de
https://doi.org/10.1016/j.cub.2022.02.073

SUMMARY

Pollen grains become increasingly independent of the mother plant as they reach maturity through poorly understood developmental programs. We report that the hormone auxin is essential during barley pollen maturation to boost the expression of genes encoding almost every step of heterotrophic energy production pathways. Accordingly, auxin is necessary for the flux of sucrose and hexoses into glycolysis and to increase the levels of pyruvate and two tricarboxylic (TCA) cycle metabolites (citrate and succinate). Moreover, bioactive auxin is synthesized by the pollen-localized enzyme HvYUCCA4, supporting that pollen grains autonomously produce auxin to stimulate a specific cellular output, energy generation, that fuels maturation processes such as starch accumulation. Our results demonstrate that auxin can shift central carbon metabolism to drive plant cell development, which suggests a direct mechanism for auxin's ability to promote growth and differentiation.

INTRODUCTION

The terminal stages of pollen development, termed maturation, ensure that pollen grains released from anthers are well equipped for successful fertilization with female gametophytes. Unicellular haploid microspores, the product of male meiosis, acquire a lytic vacuole and undergo asymmetric mitosis to produce bicellular pollen grains with a vegetative cell encasing a generative cell. In cereal crops, essential pollen maturation events include mitosis of the generative cell to produce two sperm cells and the accumulation of starch as energy reserve and of mRNA transcripts, both for later use during pollen germination and tube growth.[1,2] Pollen is strongly dependent on mother sporophytic tissues for resources, most ostensibly sugars.[3] However, the vegetative cell of maturing pollen should express its own machinery for energy generation, starch synthesis, germination, and pollen tube growth. It is not known what signals activate the timely expression of such machinery and whether those signals emanate from the sporophyte or from pollen grains themselves. MIKC*-type MADS transcription factors from rice and *Arabidopsis* are the only described gametophyte-specific regulators required for maturation.[4–6] However, it is unclear how the transcriptional programs activated by these factors in rice pollen mediate starch accumulation and other maturation processes. Similarly, the hormone jasmonate is indispensable for *Arabidopsis* pollen maturation,[7] but transcriptomics data suggest that it acts predominantly on the sporophyte, although it influences the expression of pollen-specific transporters.[8]

The hormone auxin is also necessary for postmeiotic stamen and pollen development in *Arabidopsis*. Loss of function in two auxin synthesis genes of the *YUCCA* (*YUC*) family, *AtYUC2* and *AtYUC6*, blocks the progression of pollen mitosis.[9,10] Interestingly, sporophytic microsporocytes, the progenitors of pollen grains, are the apparent source of auxin for this process.[9,10] The molecular targets regulated by auxin to allow pollen mitosis are not known. Lack of two auxin response factors (ARFs), ARF6 and ARF8, arrests late stamen development, which prevents anther opening and filament elongation[11] and results in nongerminating pollen.[12] On the other hand, a reduction in auxin synthesis or sensitivity is required to trigger anther opening and advance pollen maturation in tobacco and *Arabidopsis*.[13–15] Maturing rice anthers accumulate high levels of auxin[16,17] and express auxin synthesis and signaling genes specifically in pollen.[16] However, the primary function of this auxin wave in cereal pollen maturation is unknown, and only the detrimental effects of uncontrolled auxin accumulation on rice stamen maturation have been described.[17,18]

Starch accumulation in cereal pollen occurs in amyloplasts that differentiate from proplastids.[19,20] Starch synthesis genes that are both specific and essential to cereal pollen have been identified,[21] but how maturing pollen controls starch production remains unknown. Both transcriptional and posttranslational

Please cite this article in press as: Amanda et al., Auxin boosts energy generation pathways to fuel pollen maturation in barley, Current Biology (2022), https://doi.org/10.1016/j.cub.2022.02.073

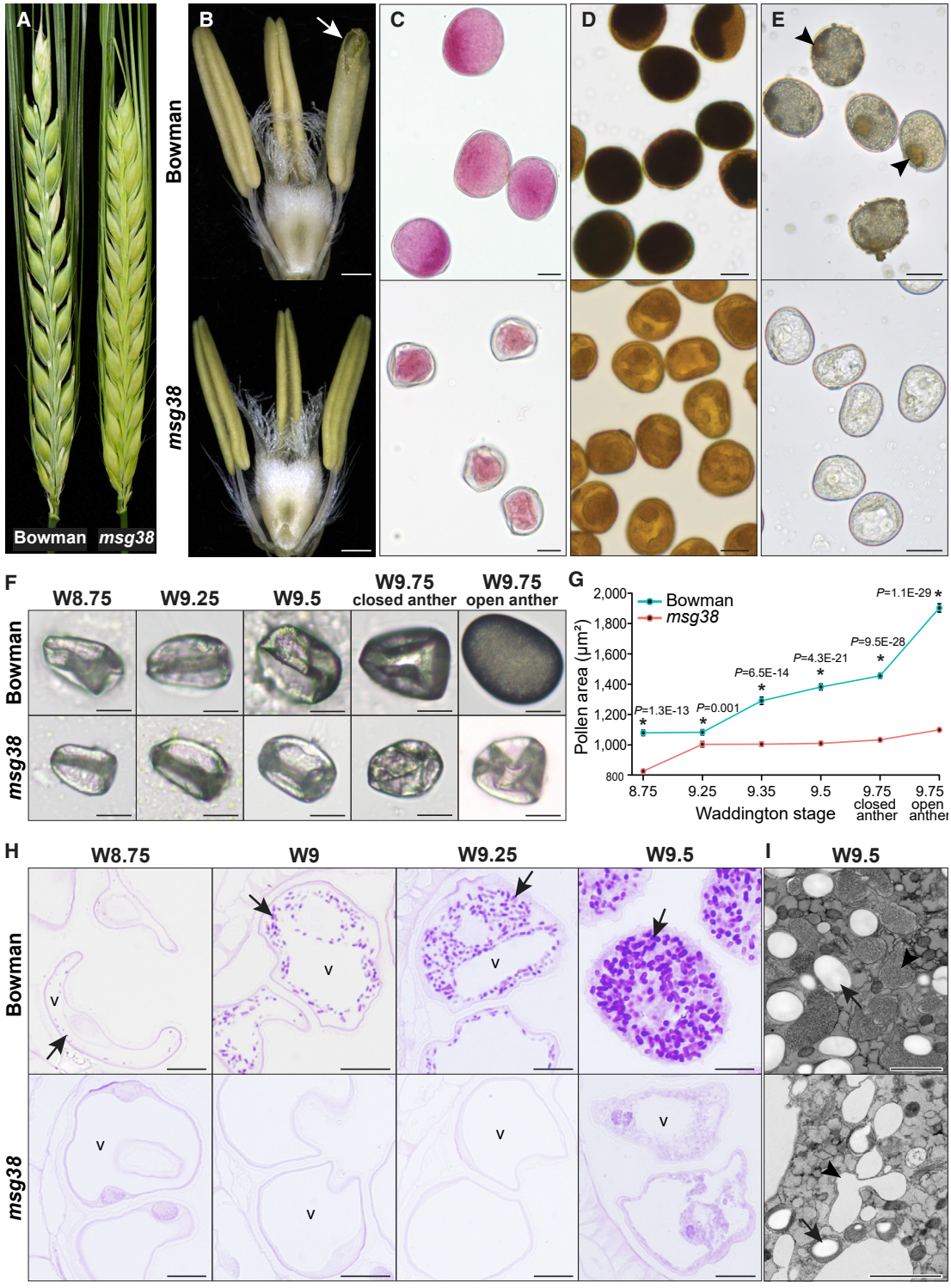

Figure 1. Phenotypic characterization of *msg38*

(A) Grain filling in Bowman and empty spikelets in *msg38* inflorescences. Scale bars, 1 cm.

(B) At stage W9.75, anther opening (arrow) occurs in Bowman but fails in *msg38*. Scale bars, 500 μm.

(C) Purple color with Alexander staining indicates viable pollen.

(D) Dark blue staining with potassium iodide reveals starch deposition only in mature Bowman pollen.

(E) Macallum's staining shows yellow potassium salt crystals (arrowheads) only in Bowman pollen. Scale bars in (C–E), 25 μm.

(F) Light micrographs of pollen visualized without liquid medium. Scale bars, 20 μm.

(legend continued on next page)

Please cite this article in press as: Amanda et al., Auxin boosts energy generation pathways to fuel pollen maturation in barley, Current Biology (2022), https://doi.org/10.1016/j.cub.2022.02.073

regulatory mechanisms of starch synthesis enzymes have been described in other nonphotosynthetic tissues such as potato tubers.[22] Moreover, ATP availability is considered the major flux determinant of starch synthesis in heterotrophic tissues,[23] and mitochondrial respiration and metabolism are believed to regulate starch production.[22] Accordingly, a high respiration rate dependent on mitochondrial oxidative phosphorylation is associated with enhanced starch buildup in lily pollen.[24–26] Thus, regulating a metabolic shift to a state of high energy production may be a mechanism to control starch accumulation in heterotrophic tissues.

To understand the mechanisms that regulate and execute pollen maturation processes, a thorough characterization of the factors involved is necessary. Here, our functional analysis of the barley gene *MALE STERILE GENETIC 38* (*MSG38*) shows that pollen grains autonomously produce auxin, which is required for a metabolic transition that fuels starch production and other processes of pollen maturation.

RESULTS

msg38 mutants are defective in pollen starch accumulation

To identify factors required for pollen maturation in temperate cereals, we use the barley collection of *msg* mutants,[27] some of which have been introgressed into the reference cultivar Bowman.[28] This includes *msg38*, which is fully sterile (Figure 1A) but without obvious defects in vegetative development (Figure S1A). According to our modified Waddington (W) scale[29] (Table S1), the morphology of *msg38* anthers progresses normally during stamen maturation (Figure S1B). However, at the stage of anther dehiscence (W9.75), anther yellowing is incomplete and opening does not occur (Figure 1B), due to delayed or failed separation of specialized septum and stomium cells (Figure S1C). *msg38* pollen appears viable but shrunken (Figures 1C and S1D) and shows no stain for starch and potassium (Figures 1D and 1E), an ion proposed to create an osmotic gradient to allow rapid pollen hydration.[30,31] Indeed, when imaged without mounting medium, maturing Bowman pollen appears dehydrated, but it expands progressively and swells spontaneously during or after anther opening (Figures 1F and 1G). Instead, *msg38* pollen stops expanding after stage W9.25, fails to swell (Figures 1F and 1G), and is unable to germinate on fertile pistils (Figure S1E).

Starch granules grow in Bowman amyloplasts from around stage W9 until W9.5, whereas the large lytic vacuole characteristic of young pollen is resorbed and replaced with multiple small vacuoles filled with electron-dense particles (Figures 1H, 1I, and S2). In contrast, no or few starch granules are visible in the plastids of *msg38* pollen, the lytic vacuole persists, and the small vacuoles appear empty (Figures 1H, 1I, and S2). All other organelles seem normal (Figure S2A), and the mutant pollen becomes tricellular with one vegetative and two sperm cells (Figure S3). Thus, *MSG38* is not required for barley pollen mitosis, but it is essential for vacuole dynamics and starch and potassium buildup during maturation. These processes likely enable pollen expansion and hydration, which in turn may increase the pressure on anther wall tissues to facilitate anther opening.

Homozygous *msg38* mutants segregate with variable, reduced frequencies in progenies of *msg38*/+ heterozygotes (16% ± 5% SD, χ^2 test p = 3.7E−72; Table S2), indicating a gametophytic defect. Accordingly, *msg38*/+ plants carry an excess of shrunken pollen (9%) and a population of small pollen (15%) not present in Bowman (Figures 2A–2C). Reciprocal test crosses with *msg38*/+ partially support a lower transmission efficiency of *msg38* in pollen (Table S3). Furthermore, grain production in *msg38*/+ plants is unaltered (Figure 2D), indicating that the *msg38* mutation does not affect the female gametophyte.

MSG38 encodes a YUCCA flavin monoxygenase involved in auxin synthesis

We identified the *MSG38* gene combining map-based cloning (Figure 3A; Data S1A) and gene variant detection in transcriptomes of *msg38* and Bowman stamens (Figure 3B). *MSG38* encodes HvYUC4, a putative flavin monoxygenase of the YUCCA (YUC) family, whose members catalyze the direct formation of the main bioactive auxin indole-3-acetic acid (IAA) from indole-3-pyruvic acid (IPyA[32,33]; Figures 3C, 3D, and S4; Data S1B). CRISPR-Cas9 editing of *HvYUC4* produced two new loss-of-function mutations, *msg38-2* and *msg38-3* (Figure 3C), that fully recapitulate the original *msg38* phenotype (Figures S5A and S5B; Tables S2 and S3). YUC proteins form four phylogenetic clades (Figure S6). MSG38/HvYUC4 is part of grass-specific subclade 2b and is a close paralog of AtYUC2 and AtYUC6 in subclade 2a (Figure 3E). In contrast to MSG38/HvYUC4, these *Arabidopsis* proteins are redundantly required for early pollen development and multiple aspects of vegetative development.[9,10] Five mutant alleles in *HvYUC2*, the barley ortholog of AtYUC2/6, do not cause obvious vegetative or reproductive defects, and *yuc2-1 msg38-2* double mutants are indistinguishable from *msg38-2* single mutants (Figures S5C–S5E). Moreover, the stamen transcriptome shows very low levels of *HvYUC2* (Data S1C). Thus, pollen development in flowering plants may generally require clade 2 YUC proteins; however, the duplication that originated group 2b YUCs may have allowed both functional specialization in reproductive development and functional divergence toward pollen maturation in grasses.

To test if MSG38/HvYUC4 participates in auxin synthesis during barley stamen maturation, we performed auxin metabolite profiling. *msg38* stamens over accumulate IPyA and its precursor L-tryptophan (Trp) at maturation stages (Figure 3F). Instead, although IAA levels increase exponentially in Bowman stamens from microspore stage (W8.25–W8.5) until pollen maturation (W9.25–W9.35), they remain low in *msg38* (Figure 3F).

(G) Mean (± SD) pollen area; n = 30 pollen grains from 3 independent inflorescences for each data point. Significant differences (asterisks) between Bowman and *msg38* at each stage determined with t test.
(H) Gradual accumulation of starch granules (arrows) detected with PAS-fuchsin. Only Bowman pollen resorbs the lytic vacuole (v). Scale bars, 10 μm.
(I) Representative transmission electron micrographs of mature pollen with starch granules (arrows) and small vacuoles (arrowheads). Scale bars, 2 μm.
See also Figures S1–S3 and Table S1.

Please cite this article in press as: Amanda et al., Auxin boosts energy generation pathways to fuel pollen maturation in barley, Current Biology (2022), https://doi.org/10.1016/j.cub.2022.02.073

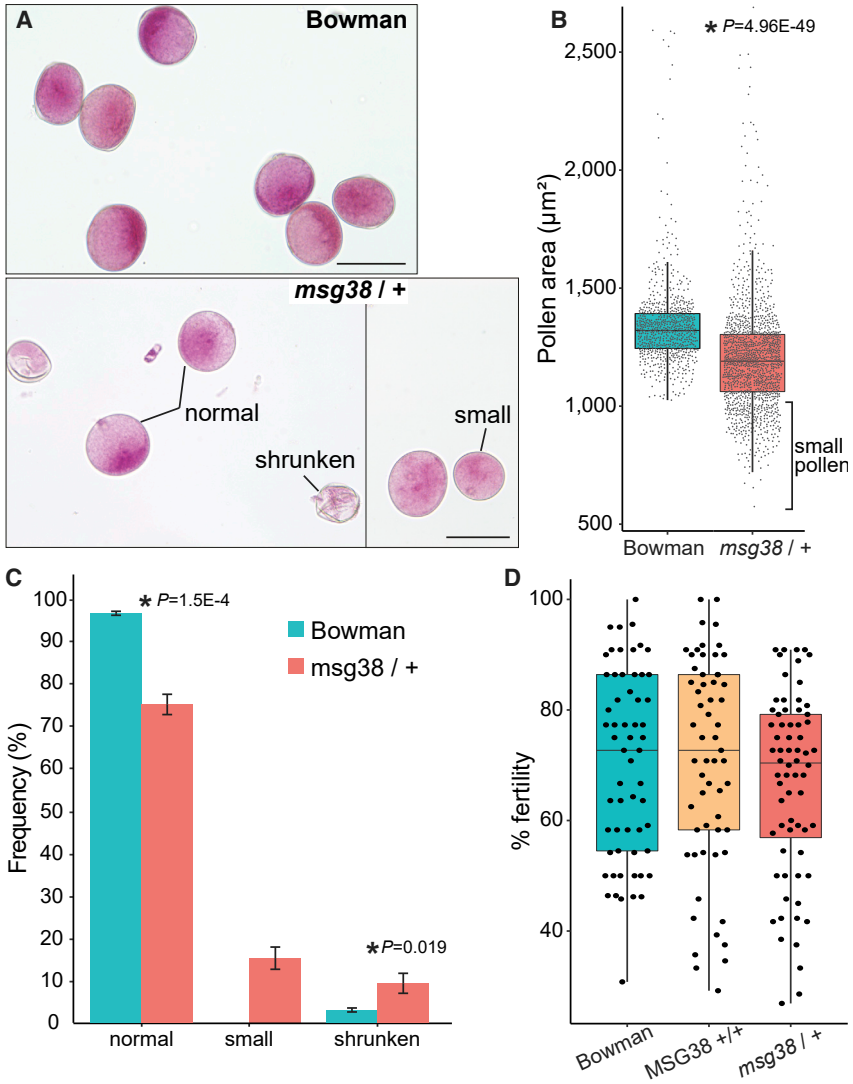

Figure 2. Pollen morphology and fertility of heterozygous *msg38*/+

(A) Pollen visualized with Alexander's stain. *msg38*/+ plants carry three pollen morphologies: normal, small, and shrunken, whereas most Bowman pollen is normal with a low frequency of shrunken pollen. Scale bars, 50 µm.

(B) Area quantification in regular-shaped pollen grains. Shrunken pollen not considered. Box plot whiskers represent ±1.5× the interquartile range; horizontal lines, medians; dots, individual measurements. The subpopulation of small pollen in *msg38*/+ causes a significant difference (asterisk) in the mean pollen size when compared with Bowman, as determined with t test. n = 710 (Bowman) and 1,294 (*msg38*/+) pollen grains obtained from six independent inflorescences per genotype.

(C) Mean frequency (±SD) of pollen types in 6 inflorescences per genotype. Significant differences (asterisks) determined with t tests.

(D) Fertility (number of grains divided by the number of spikelets per inflorescence) under greenhouse conditions in three genotypes: Bowman and wild-type siblings in segregating populations (homozygous MSG38+/+ and heterozygous *msg38*/+). No significant difference between the genotypes with one-way ANOVA test (p = 0.37). Number of inflorescences quantified per genotype = 59 (Bowman and MSG38+/+) and 68 (*msg38*/+). Box plot features as in (A).

See also Tables S2 and S3.

ox-IAA and three other IAA degradation products also follow this pattern (Figure 3F; Data S1D). Thus, MSG38/HvYUC4 catalyzes the direct formation of IAA during barley stamen maturation. Noticeably, oxIAA and oxIAA-Glc in Bowman stamens accumulate to ~50–100 times higher levels than IAA, the highest of all detected auxin metabolites, indicating a rapid degradation of the active hormone (Figure 3F; Data S1D).

MSG38/HvYUC4 is a pollen-specific protein

MSG38/*HvYUC4* transcripts are undetectable in vegetative tissues and in inflorescences with meiotic stamens (W6–W7.5). They appear first in Bowman reproductive organs at W8, increase in stamens exponentially like IAA, peak around W9.25, and decline rapidly afterward (Figure 4A). Thus, *MSG38*/*HvYUC4* functions specifically in reproductive tissues within a limited time window. Although *MSG38*/*HvYUC4* transcripts are also detected at W8 in *msg38* mutant tissue, they only increase by one order of magnitude and are still detectable at W9.5–W9.75 (Figure 4A), indicating that auxin exerts feedback regulation on a gene associated with its own synthesis.

In situ localization first detects *MSG38*/*HvYUC4* transcripts in W9 anthers, mainly in pollen grains and vascular tissues and less strongly in the endothecium (Figure 4B). However, an MSG38-fluorescent protein fusion driven by a 3-kb *MSG38*/*HvYUC4* endogenous promoter localizes exclusively in pollen, also from W9 onwards (Figure 4C), and restores the fertility of *msg38-2* mutants (Figure 4D). Thus, MSG38/HvYUC4 functions solely in pollen grains to catalyze local auxin production and drive pollen maturation. In this scenario, no auxin import from sporophytic tissues is required, in agreement with the gametophytic nature of the *msg38* mutation. We hypothesize that auxin exported from wild-type pollen in *msg38*/+ heterozygotes is imported into mutant *msg38* pollen, which can then develop normally or with varied success, explaining the relatively high yet reduced, variable transmission of *msg38* from pollen (Tables S2 and S3). This contrasts with other knockout gametophytic mutations, where no or very few homozygous mutants can be recovered.[21]

MSG38/HvYUCCA4 is required to boost energy metabolism during pollen maturation

The *msg38* mutant defects mainly concern pollen grains after stage W9, coinciding with the beginning of starch formation. Moreover, MSG38-fluorescent protein fusions are first found only from stage W9, and we detected the highest levels of

Please cite this article in press as: Amanda et al., Auxin boosts energy generation pathways to fuel pollen maturation in barley, Current Biology (2022), https://doi.org/10.1016/j.cub.2022.02.073

CellPress

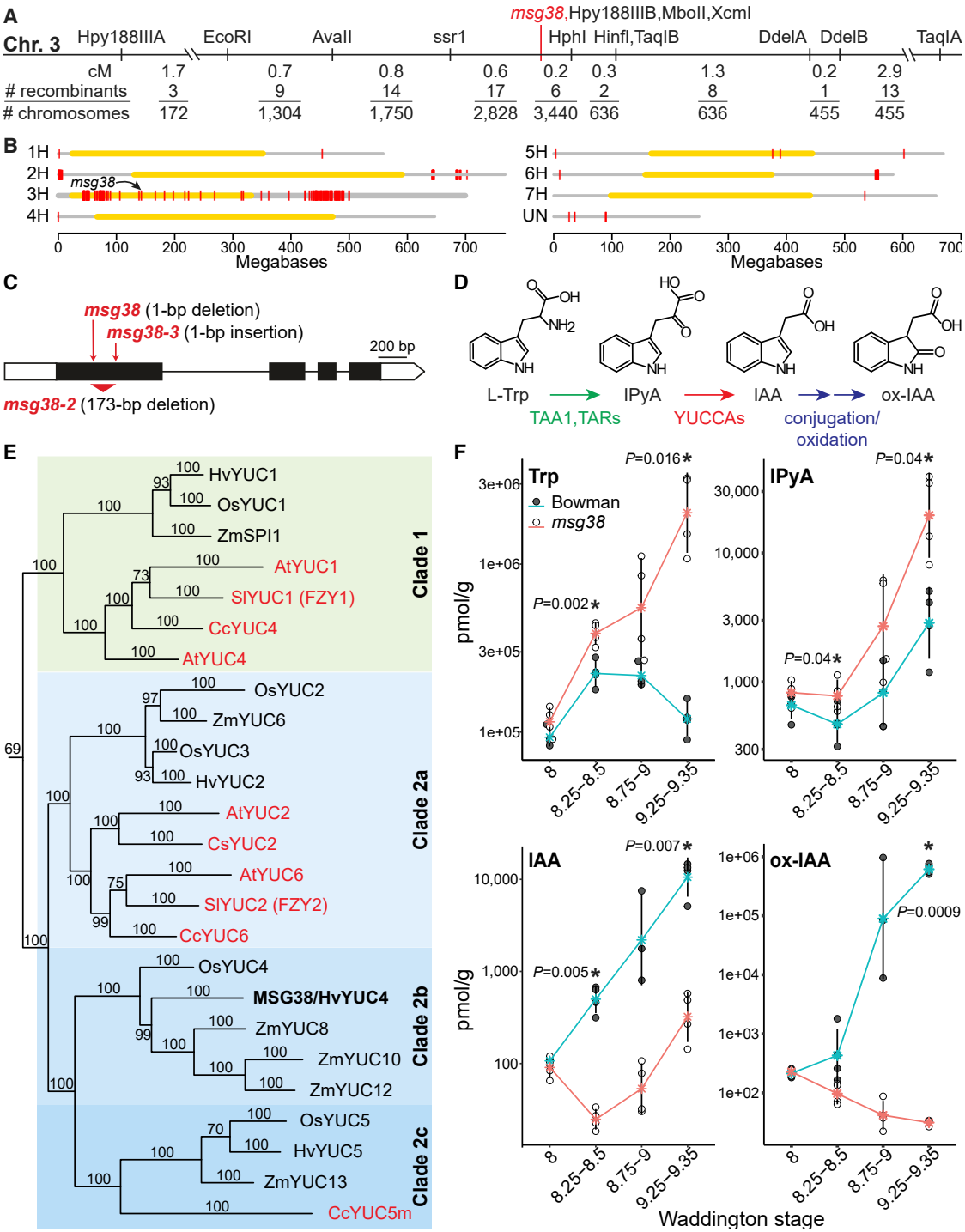

Figure 3. *MSG38* encodes a YUCCA flavin monoxygenase involved in auxin synthesis

(A) Genetic map of the *msg38* locus in a 0.8 cM interval of barley chromosome 3. See marker information in Data S1A.

(B) Location of RNA-seq polymorphisms detected between Bowman and *msg38* (red bars), with the *msg38* gene variant indicated. See STAR Methods for how this variant was identified as unique to *msg38*. Note that the majority of polymorphisms are part of chromosome 3, indicating that most other chromosomal regions carry a Bowman background. Yellow, approximate location of pericentromeric regions.

(C) Structure of *MSG38/HvYUC4* gene and location of the three *msg38* mutant alleles (red). Boxes depict exons (coding regions in black, untranslated regions in white).

(D) Biosynthesis and degradation of bioactive IAA.

(E) Phylogeny of closest MSG38/HvYUC4 relatives. Monocot, black; eudicot, red. Numbers are node posterior probabilities. See Data S1B and S2 for protein sequence information.

(legend continued on next page)

Please cite this article in press as: Amanda et al., Auxin boosts energy generation pathways to fuel pollen maturation in barley, Current Biology (2022), https://doi.org/10.1016/j.cub.2022.02.073

bioactive auxin at stages W9.25 and W9.35. Thus, we compared the transcriptomes of *msg38* and Bowman stamens at W9.25 and W9.35 to identify potential targets of auxin signaling that carry out pollen maturation (Figures 5A and 5B; Data S1C and S1E). Differentially expressed genes (DEGs, |fold change (FC)| $\geq$ 1.5; FDR-adjusted p $\leq$ 0.05) form six clusters (Figures 5C and 5D; Data S1E). Most DEGs (64%) are downregulated in *msg38* and fall in clusters 1 and 2. Cluster 1 contains genes more strongly expressed at W9.25 than W9.35 in Bowman, such as *MSG38/HvYUC4*, and is enriched for auxin-responsive genes (Data S1F and S1G). More noticeably, it includes genes encoding almost every step of canonical heterotrophic ATP generation: from sugar transport and degradation to ATP synthase activity (Figure 6A; Data S1F, S1H, and S1I). qRT-PCR confirmed coexpression of *Hexokinase5* (glycolysis) and *Cytochrome c* (oxidative phosphorylation) with *MSG38/HvYUC4* (Figure 6B). *msg38* stamens show downregulation of only three starch synthesis genes, including *AGP-L1*, a subunit in the first committed step of the pathway[22] (Figures 6A and 6B; Data S1I). Machine learning predicts that, similar to auxin-responsive genes, most energy and starch metabolism genes downregulated in *msg38* carry putative upstream binding sites to ARFs, the transcriptional regulators effecting auxin responses (Figures 6C and 6D; Data S1J). Metabolite profiling (Data S1K) shows that *msg38* stamens at W9.35 tend to over accumulate sucrose, glucose, and fructose (Figure 6E). Thus, auxin signaling is not required for photosynthate import into stamens but rather for both sucrose breakdown and normal flux through glycolysis. Accordingly, *msg38* stamens contain lower levels of pyruvate, the output of glycolysis, and of citrate and succinate, two important metabolites of the TCA cycle (Figure 6E). Ultimately, mutant stamens contain ~7 times less starch than Bowman's (Figure 6F). Overall, the data support that auxin promotes starch synthesis in barley pollen mainly by boosting the expression of genes required for energy generation. We conclude that this boost shifts pollen metabolism to a high energy production state to support the demand for ATP, the predominant factor driving starch synthesis in heterotrophic tissues.[23]

An excess of genes encoding starch degradation enzymes, transporters, and cytoskeleton and signal transduction components are also downregulated in *msg38* (Figure 6A; Data S1F, S1I, and S1L). These genes are typical of mature pollen transcriptomes and likely part of a transcript pool stored for use after pollen release,[2] including homologs of known factors of pollen hydration and tube growth (Data S1M). Several of these gene categories are enriched in cluster 2, where transcripts reach higher levels at W9.35 than W9.25 in Bowman (Figures 5C and 5D; Data S1F), suggesting that auxin induces them in a second gene expression wave, close to the completion of maturation.

DISCUSSION

As cells progress through development, their demand for energy and building blocks also changes. Thus, shifts in the flux of metabolic pathways are required during developmental progressions to support such varying demands.[34] Hormones and transcriptional regulators that effect metabolic transitions in developing animal cells are well documented, particularly for the switch to aerobic glycolysis that characterizes proliferating cells.[35,36] In contrast, mechanisms of metabolic reprogramming during normal plant development are just emerging.[37,38] Here, we show that the timely accumulation of auxin can shift central carbon metabolism to drive the development of a specific cell type. We propose that auxin may also activate similar metabolic shifts in other processes requiring a high energy production state, such as that reported for starch accumulation during barley grain development.[39] In fact, auxin is required for starch buildup in maize kernels and pea seeds; however, this auxin requirement was linked until now only to the activation of starch synthesis genes[40,41] and to an influence in sucrose import or utilization.[40]

Our results also show that barley pollen autonomously produce large amounts of auxin, whose primary function is to activate a gene expression program directly linked to concrete cellular outputs such as energy production. We hypothesize that once pollen receives enough sucrose from the mother plant, auxin ensures the completion of pollen development into a dehydrated structure that stores energy in the form of starch, ready for its terminal functions, germination, tube growth, and fertilization.

Our work provides mechanistic support to classical physiological experiments showing that auxin promotes mitochondrial respiration as prerequisite for cell growth and division.[42,43] We hypothesize that shifting the flux of central carbon metabolism may be a general function of auxin to allow cell growth or differentiation. A similar hypothesis was raised before,[44] but no mechanism was envisioned. Moreover, the pleiotropic effects of other auxin-deficient mutants prevented separating a putative direct role of auxin in metabolism from its function in the development of basic structures such as leaf stomata and veins, which are themselves necessary for normal carbon metabolism.[44] We also propose that, in addition to the obvious effect that energy and building block acquisition may have in organ growth, differences in energy metabolism may potentiate the fate of differentiating cells. Thus, auxin may not simply instruct cells to acquire a fate but may also actively modify their metabolism so that the specific bioenergetic demands of that fate are met.

The emerging mechanisms of metabolic reprogramming known in plants so far concern nutrient perception[37,38] and abiotic stress responses.[45] For example, the kinases SNF1-RELATED (SnrK1) and TARGET OF RAPAMYCIN (TOR) integrate energy status or sugar availability to dynamically adjust plant metabolism via posttranslational modification of primary metabolism enzymes[46] or nuclear gene expression factors.[37] Responses to nutrients or abiotic stress often involve activation of hormone signaling, presumably to optimize plastic

(F) Quantification of auxin-related metabolites in Bowman and *msg38* inflorescences (W8) and stamens (all other stages). Small circles are individual measurements; color lines connect means (color stars); black lines, ±1 SD. n = 4 except for Bowman W8.75–W9 (n = 3). Black asterisks indicate significant differences between Bowman and *msg38* at a given stage determined with one-tailed t tests. See Data S1D.
See also Figures S4–S6.

Please cite this article in press as: Amanda et al., Auxin boosts energy generation pathways to fuel pollen maturation in barley, Current Biology (2022), https://doi.org/10.1016/j.cub.2022.02.073

CellPress

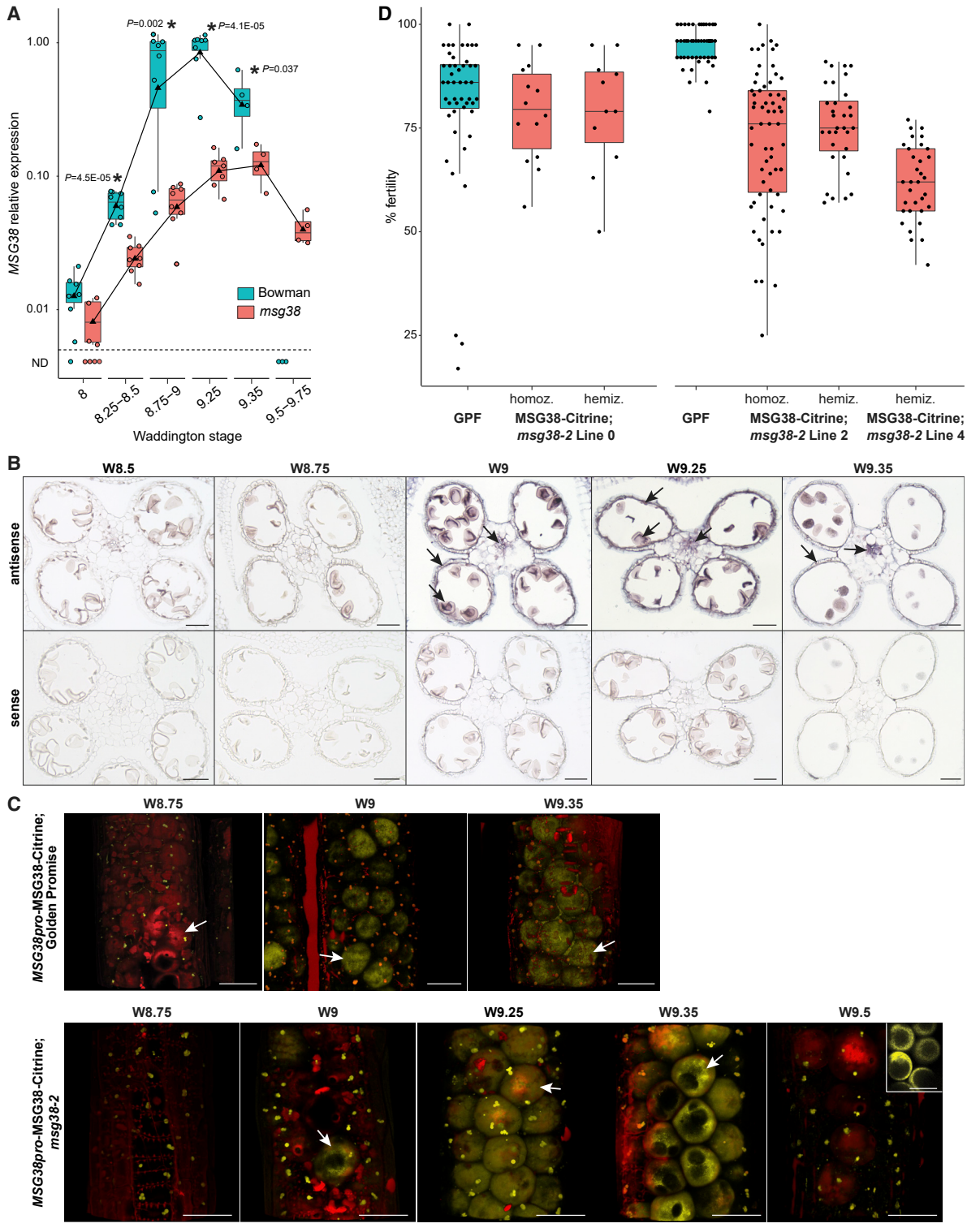

Figure 4. Expression of *MSG38/HvYUC4* during pollen maturation

(A) qRT-PCR of *MSG38/HvYUC4* in pooled stamens and pistils (W8) and stamens (all other stages). Samples below dotted line, not detectable (ND). Data pooled from two independent experiments: n = 4 for W9.35 and W9.5–9.75, except Bowman W9.5–9.75 (n = 3); for all other stages, n = 8, except *msg38* W9.25 (n = 7). Box plot whiskers represent ±1.5× the interquartile range; horizontal lines, medians; black triangles, means; small circles, individual measurements. Asterisks indicate significant differences between Bowman and *msg38* at a given stage determined with one-tailed t tests.

(B) *MSG38/HvYUC4* RNA *in situ* hybridization in Bowman anthers. Arrows point to positive purple signals in pollen, vasculature, and endothecium.

(legend continued on next page)

Please cite this article in press as: Amanda et al., Auxin boosts energy generation pathways to fuel pollen maturation in barley, Current Biology (2022), https://doi.org/10.1016/j.cub.2022.02.073

growth.[47] Therefore, a function of auxin, and potentially other hormones, in effecting metabolic transitions would also provide a direct mechanism for controlling plant development in response to those external stimuli. Importantly, this would also suggest that hormone signaling could directly adapt metabolism to the conditions imposed by stress or nutrient availability.

Sugar accumulation is a prerequisite of starch synthesis in cereal pollen[3], but according to our data, it occurs independently of auxin. Thus, it is possible that sugar import into pollen both precedes and triggers auxin synthesis to enable the metabolic switch required for starch production. In this scenario, SnrK1, TOR, or other sugar perception mechanism could promote the expression of *MSG38/HvYUC4* in response to sugar levels. Accordingly, SnrK1 is necessary for starch accumulation in barley pollen.[48] On the other hand, it is also formally possible that auxin exerts its effect on energy metabolism more indirectly via activation of SnRK1 or TOR signaling.

In *Arabidopsis*, auxin is necessary before the first microspore mitosis,[10] an earlier stage of pollen development that coincides with the initiation of a transient buildup of starch granules.[49] This suggests the intriguing possibility that *Arabidopsis* pollen also uses auxin to promote starch formation with a transcriptional program similar to barley but with different timing.

Several aspects of plant development rely on auxin gradients generated cooperatively by local auxin synthesis and long-distance polar transport from buds or young organs.[50] Instead, early genetic and expression analyses in *Arabidopsis* already suggested that anthers themselves are the main source of auxin during stamen maturation.[13,14] Later work showed more specifically that young *Arabidopsis* pollen grains rely on auxin produced by their progenitor sporophytic microsporocytes.[9,10] This and our findings with barley pollen suggest that in flowering plants the male gametophyte (or its immediate progenitor) autonomously produce auxin to drive its own development. Still, other evidence suggests that auxin transport is also important for stamen maturation in *Arabidopsis*. First, translocation from anthers to filaments may promote filament elongation.[14] Second, normal pollen maturation, anther opening, and filament elongation require auxin transport from the tapetum to the middle layer[51]; such a gradient could potentially serve as a signaling attenuation mechanism. Our data show that MSG38/HvYUC4 in pollen is responsible for the bulk of auxin synthesis in maturing barley stamens. It remains to be determined if auxin translocation from barley pollen to the anther sac or other tissues creates any gradients and if these have a biological function. However, normal filament elongation in the *msg38* mutant (Figure S1B) indicates that auxin from pollen is not necessary for this process in barley.

MSG38/HvYUC4 specifically catalyzes auxin synthesis in maturing barley stamens without apparently participating in other plant processes. It is likely that its orthologs in YUC subclade 2b, composed of grass-only members, perform the same specific function. Thus, one can envision targeted chemical inhibition of these YUCs to induce male sterility without affecting plant performance and, as such, represents a novel strategy for large-scale hybrid seed production in crop cereals.

STAR★METHODS

Detailed methods are provided in the online version of this paper and include the following:

- KEY RESOURCES TABLE
- RESOURCE AVAILABILITY
  - Lead contact
  - Materials availability
  - Data and code availability
- EXPERIMENTAL MODEL AND SUBJECT DETAILS
  - Plant material
  - Plant genotyping
  - Growth conditions
- METHOD DETAILS
  - Stamen and pistil imaging
  - Light microscopy
  - Anther histology
  - Pollen viability assay with Alexander's staining
  - Detection of pollen starch with light microscopy
  - Detection of potassium salt crystals in pollen
  - Area of fresh pollen without mounting medium
  - Scanning electron microscopy
  - Pollen germination assay
  - Pollen nuclei visualization with DAPI staining
  - Transmission electron microscopy
  - *MSG38* gene identification
  - Phylogenetic analysis
  - *Agrobacterium*-mediated stable plant transformation
  - Gene editing
  - Auxin metabolite profiling
  - RNA Extraction and qRT-PCR
  - RNA *in situ* hybridization
  - *MSG38pro*-MSG38-Citrine reporter lines
  - Transcriptome analysis
  - Prediction of auxin response factor (ARF) binding sites with a machine learning model

(C) MSG38g-Citrine fluorescent protein (yellow) in anthers of cultivar Golden Promise Fast (*MSG38* +/+, upper) or of *msg38-2* homozygous mutants (lower). Samples contrasted with propidium iodide (red). Arrows, pollen grains. Inset in lower panel shows fluorescence signal in pollen extracted from anthers at W9.5; at this stage, the confocal microscope is not able to image into pollen grains inside anthers. Small yellow/orange dots are autofluorescent structures of unknown origin. Scale bars in (B) and (C), 50 μm.

(D) Fertility (number of grains divided by the number of spikelets per inflorescence) in cultivar Golden Promise Fast (GPF) and three independent MSG38g-Citrine fluorescent protein reporter lines introgressed into the *msg38-2* mutant background. The fusion protein rescues the fertility of the otherwise fully sterile mutant. Dots represent fertility of individual inflorescences. For each line, we scored a number of inflorescences (n) derived from a number of plants (m), as follows: GPF (left, 48/10), line 0 (25/7), GPF (right, 50/5), line 2 (95/9), and line 4 (33/3). Homozygous or hemizygous refers to the apparent configuration of the transgenic reporter in plants from segregating populations. Box plots as in Figure 2A.

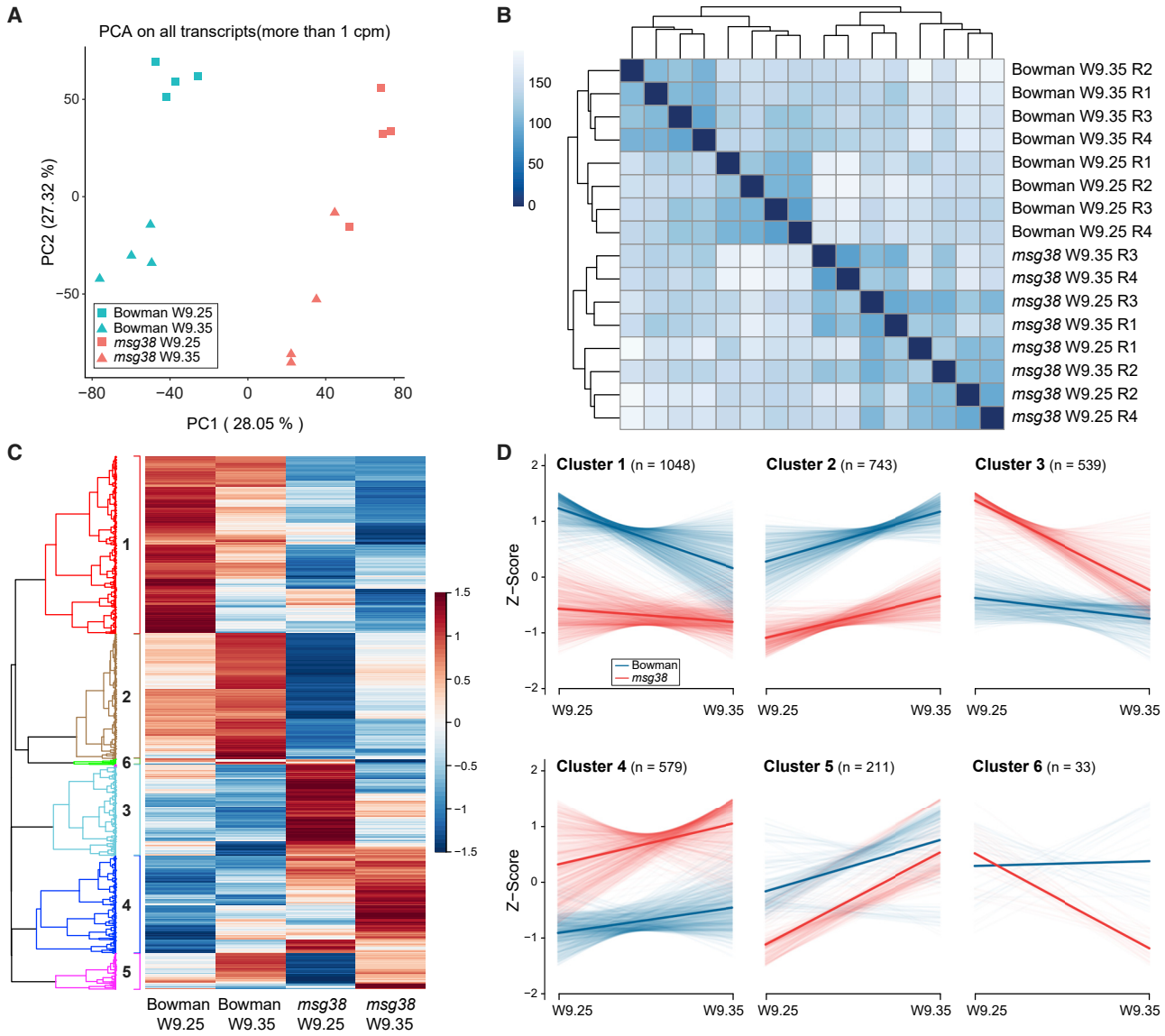

Figure 5. Transcriptomic analysis of Bowman and *msg38* stamens at stages W9.25 and W9.35

(A) Principal component analysis of normalized expression levels (counts per million, cpm) of all expressed genes.

(B) Heatmap of Euclidean distances between samples calculated from normalized cpm values of all expressed genes. In (A and B), we analyzed the data of all 16 biological replicates (4 per genotype and stage). As expected from the experiment design, replicates group by genotype and stage in both analyses. However, two *msg38* replicates (W9.25 R3 and W9.35 R2) appeared more distant from their expected groups. Thus, they were excluded from all differential expression analyses.

(C) Hierarchical clustering of DEGs. Scale: $\log_2$ mean-centered counts per million.

(D) Expression profiles of 3,153 differentially expressed genes grouped in six coexpression clusters identified with hierarchical clustering. *Z* scores are the mean-centered and scaled transcript levels in cpm. Within each cluster, the *Z* scores of individual transcripts at W9.25 and W9.35 stages are connected by light-colored thin lines, whereas the thicker dark-colored line connects the mean *Z* scores across all transcripts at both stages. Sixty four percent of DEGs are downregulated in *msg38*, most forming clusters 1 and 2, whereas the majority of *msg38* upregulated transcripts are part of clusters 3 and 4. The smaller clusters 5 and 6 contain mainly transcripts downregulated in *msg38*.

See also Data S1C, S1E–S1I, S1L, and S1M.

- ○ Metabolite profiling and starch measurements
- ● QUANTIFICATION AND STATISTICAL ANALYSIS

SUPPLEMENTAL INFORMATION

Supplemental information can be found online at https://doi.org/10.1016/j.cub.2022.02.073.

ACKNOWLEDGMENTS

We thank E. Wendeler, S. Höhmann, I. Rouhara, C. Dawidson, and A. Oehl for excellent technical support; GRIN-USDA for maintaining the *msg* mutant collection and F. Salamini for first propagating it at our institute; R. Franzen for scanning electron microscopy; R. Lange and M. R. Herma for running some R scripts; R. Schwacke for ARAMEMNON's rice transporter list; the Swedish Metabolomics Centre for access to instrumentation; G. W. van

Please cite this article in press as: Amanda et al., Auxin boosts energy generation pathways to fuel pollen maturation in barley, Current Biology (2022), https://doi.org/10.1016/j.cub.2022.02.073

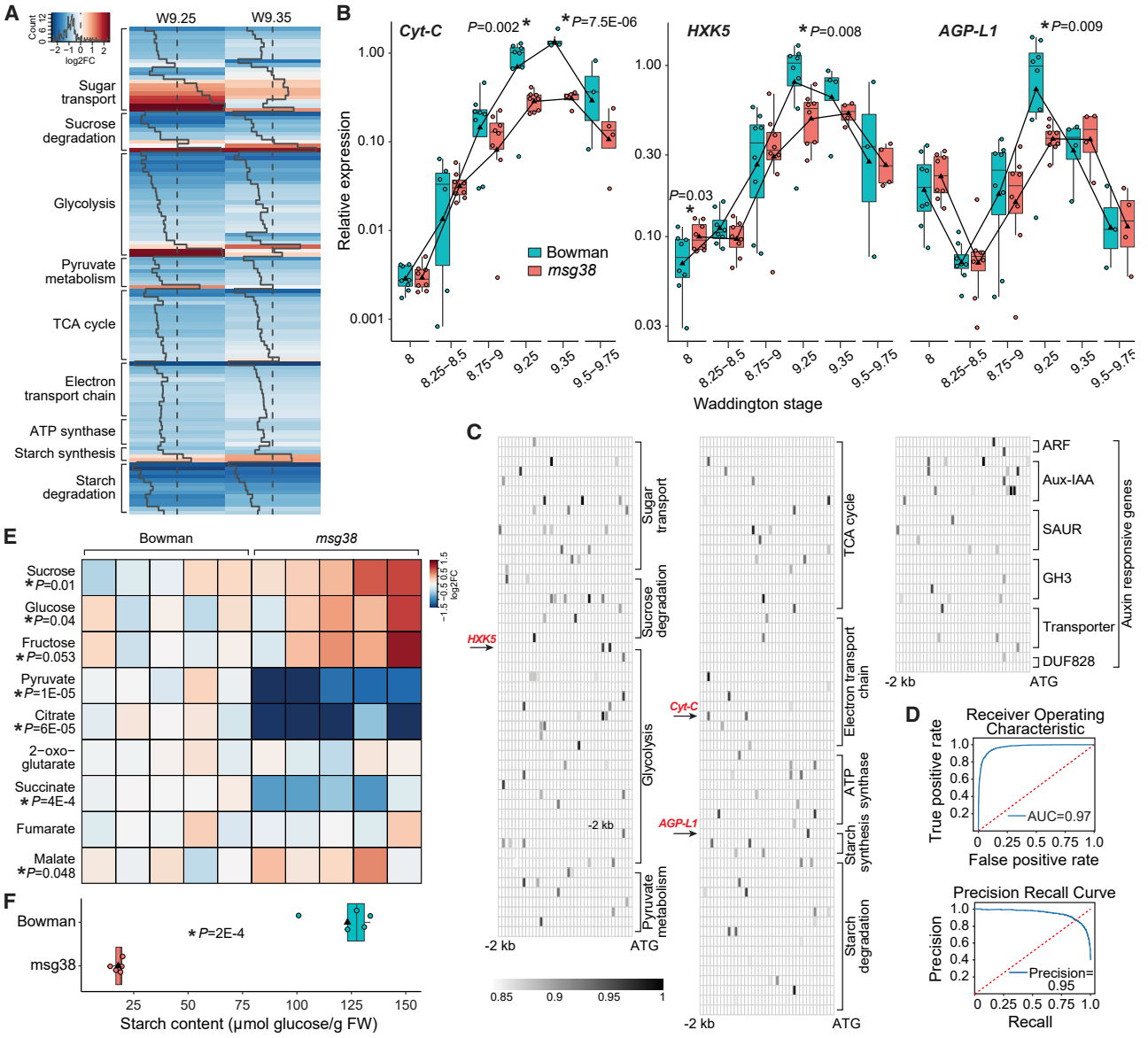

Figure 6. Auxin boosts energy metabolism in barley stamens

(A) $\log_2$ FC of DEGs involved in ATP and starch metabolism. Gray solid trace shows FC values for each gene relative to $\log_2$ FC = 0 (dotted gray lines).

(B) qRT-PCR of representative DEGs. Samples, box plots, and statistics as in Figure 4A.

(C) Significant scores (>0.85) of model-predicted ARF binding sites within 53-bp fragments (boxes) in 2-kb regions upstream of ATP/starch metabolism and auxin-responsive genes downregulated in *msg38*. Genes tested in (B) are indicated in red.

(D) Machine learning bag-of-k-mer ZmARF35 model. The receiver operating characteristic (ROC) plot indicates that the predictions of the ZmARF35 machine learning model are 97% correct as measured by the area under the ROC curve (AUC). (F) The precision-recall curve shows that the precision of the model's predictions is 95%.

(E) Log_2 relative levels of sucrose, hexoses, pyruvate, and TCA cycle organic acids in five biological replicates of Bowman and *msg38* stamens at stage W9.35. Relative levels calculated from the ratio of normalized values of each replicate to the mean of normalized values of all five Bowman replicates. Asterisks indicate significant differences between the mean of Bowman and *msg38* values determined with one-tailed t test.

(F) Starch levels in the same samples of (E) are significantly lower in *msg38* as determined with one-tailed t test. Box plot as in Figure 4A, except that medians are vertical lines.

See also Data S1E–S1M.

Esse, A. Walla, X. Bi, J. Zhong, and M. von Korff for discussions and for sharing the Golden Promise Fast line, barley RNA-seq data, scripts, and GO annotations; and C. Gutjahr, P. Schulze-Lefert, and M. Tsiantis for comments on the manuscript. This work was supported by the Max Planck Society (I.F.A. and A.R.F.); the Swedish Foundation for Strategic Research, Vinnova (K.L.); the Knut and Alice Wallenberg Foundation, KAW (K.L.); the Swedish Research Council VR (K.L.); the European Union's Horizon 2020 research and innovation programme (grants SGA-CSA 664621 and 739582 under FPA664620 to A.R.F.); and the National Science Foundation (grant IOS-1546873 to A.G.).

AUTHOR CONTRIBUTIONS

Conceptualization, I.F.A.; data curation, I.F.A. and F.P.F.; formal analysis, D.A., F.P.F., U.N., J.Š., Y.Z., Z.C., and I.F.A.; funding acquisition, I.F.A., K.L., A.R.F., and A.G.; investigation, D.A., F.F., U.N., M.P., J.Š., Y.Z., Z.C., and I.F.A.; supervision, I.F.A., K.L., A.R.F., and A.G.; visualization, D.A. and I.F.A.; writing—original draft, I.F.A.; writing—review & editing, I.F.A. with input from all authors.

DECLARATION OF INTERESTS

The authors declare no competing interests.

INCLUSION AND DIVERSITY

One or more of the authors of this paper self-identifies as an underrepresented ethnic minority in science.

Received: December 21, 2021
Revised: February 22, 2022
Accepted: February 24, 2022
Published: March 21, 2022

REFERENCES

1. Christensen, J.E., Horner, H.T., and Lersten, N.R. (1972). Pollen wall and tapetalorbicularwalldevelopment in *Sorghum bicolor* (Gramineae). Am.J.Bot. *59*, 43–58. https://doi.org/10.2307/2441229.
2. Rutley, N., and Twell, D. (2015). A decade of pollen transcriptomics. Plant Reprod. *28*, 73–89. https://doi.org/10.1007/s00497-015-0261-7.
3. Zhang, H., Liang, W., Yang, X., Luo, X., Jiang, N., Ma, H., and Zhang, D. (2010). Carbon starved anther encodes a MYB domain protein that regulates sugar partitioning required for rice pollen development. Plant Cell *22*, 672–689. https://doi.org/10.1105/tpc.109.073668.
4. Adamczyk, B.J., and Fernandez, D.E. (2009). MIKC* MADS domain heterodimers are required for pollen maturation and tube growth in *Arabidopsis*. Plant Physiol. *149*, 1713–1723. https://doi.org/10.1104/pp.109.135806.
5. Liu, Y., Cui, S., Wu, F., Yan, S., Lin, X., Du, X., Chong, K., Schilling, S., Theißen, G., and Meng, Z. (2013). Functional conservation of MIKC*-Type MADS box genes in *Arabidopsis* and rice pollen maturation. Plant Cell *25*, 1288–1303. https://doi.org/10.1105/tpc.113.110049.
6. Verelst, W., Twell, D., de Folter, S., Immink, R., Saedler, H., and Münster, T. (2007). MADS-complexes regulate transcriptome dynamics during pollen maturation. Genome Biol. *8*, R249. https://doi.org/10.1186/gb-2007-8-11-r249.
7. McConn, M., and Browse, J. (1996). The critical requirement for linolenic acid is pollen development, not photosynthesis, in an Arabidopsis mutant. Plant Cell *8*, 403–416.
8. Mandaokar, A., Thines, B., Shin, B., Lange, B.M., Choi, G., Koo, Y.J., Yoo, Y.J., Choi, Y.D., Choi, G., and Browse, J. (2006). Transcriptional regulators of stamen development in Arabidopsis identified by transcriptional profiling. Plant J. *46*, 984–1008. https://doi.org/10.1111/j.1365-313X.2006.02756.x.
9. Cheng, Y., Dai, X., and Zhao, Y. (2006). Auxin biosynthesis by the YUCCA flavin monooxygenases controls the formation of floral organs and vascular tissues in *Arabidopsis*. Genes Dev. *20*, 1790–1799. https://doi.org/10.1101/gad.1415106.
10. Yao, X., Tian, L., Yang, J., Zhao, Y.N., Zhu, Y.X., Dai, X., Zhao, Y., and Yang, Z.N. (2018). Auxin production in diploid microsporocytes is necessary and sufficient for early stages of pollen development. PLoS Genet. *14*, e1007397. https://doi.org/10.1371/journal.pgen.1007397.
11. Nagpal, P., Ellis, C.M., Weber, H., Ploense, S.E., Barkawi, L.S., Guilfoyle, T.J., Hagen, G., Alonso, J.M., Cohen, J.D., Farmer, E.E., et al. (2005). Auxin response factors ARF6 and ARF8 promote jasmonic acid production and flower maturation. Development *132*, 4107–4118. https://doi.org/10.1242/dev.01955.
12. Ru, P., Xu, L., Ma, H., and Huang, H. (2006). Plant fertility defects induced by the enhanced expression of microRNA167. Cell Res. *16*, 457–465. https://doi.org/10.1038/sj.cr.7310057.
13. Cecchetti, V., Altamura, M.M., Brunetti, P., Petrocelli, V., Falasca, G., Ljung, K., Costantino, P., and Cardarelli, M. (2013). Auxin controls *Arabidopsis* anther dehiscence by regulating endothecium lignification and jasmonic acid biosynthesis. Plant J. *74*, 411–422. https://doi.org/10.1111/tpj.12130.
14. Cecchetti, V., Altamura, M.M., Falasca, G., Costantino, P., and Cardarelli, M. (2008). Auxin regulates *Arabidopsis* anther dehiscence, pollen maturation, and filament elongation. Plant Cell *20*, 1760–1774. https://doi.org/10.1105/tpc.107.057570.
15. Cecchetti, V., Pomponi, M., Altamura, M.M., Pezzotti, M., Marsilio, S., D'Angeli, S., Tornielli, G.B., Costantino, P., and Cardarelli, M. (2004). Expression of rolB in tobacco flowers affects the coordinated processes of anther dehiscence and style elongation. Plant J. *38*, 512–525. https://doi.org/10.1111/j.0960-7412.2004.02064.x.
16. Hirano, K., Aya, K., Hobo, T., Sakakibara, H., Kojima, M., Shim, R.A., Hasegawa, Y., Ueguchi-Tanaka, M., and Matsuoka, M. (2008). Comprehensive transcriptome analysis of phytohormone biosynthesis and signaling genes in microspore/pollen and tapetum of rice. Plant Cell Physiol. *49*, 1429–1450. https://doi.org/10.1093/pcp/pcn123.
17. Song, S., Chen, Y., Liu, L., See, Y.H.B., Mao, C., Gan, Y., and Yu, H. (2018). OsFTIP7 determines auxin-mediated anther dehiscence in rice. Nat. Plants *4*, 495–504. https://doi.org/10.1038/s41477-018-0175-0.
18. Zhao, Z., Zhang, Y., Liu, X., Zhang, X., Liu, S., Yu, X., Ren, Y., Zheng, X., Zhou, K., Jiang, L., et al. (2013). A role for a dioxygenase in auxin metabolism and reproductive development in rice. Dev. Cell *27*, 113–122. https://doi.org/10.1016/j.devcel.2013.09.005.
19. Clément, C., and Pacini, E. (2001). Anther plastids in angiosperms. Bot.Rev. *67*, 54–73. https://doi.org/10.1007/BF02857849.
20. Pacini, E., Taylor, P.E., Singh, M.B., and Knox, R.B. (1992). Development of plastids in pollen and tapetum of rye-grass, *Lolium perenne* L. Ann.Bot. *70*, 179–188. https://doi.org/10.1093/oxfordjournals.aob.a088455.
21. Lee, S.K., Eom, J.S., Hwang, S.K., Shin, D., An, G., Okita, T.W., and Jeon, J.S. (2016). Plastidic phosphoglucomutase and ADP-glucose pyrophosphorylase mutants impair starch synthesis in rice pollen grains and cause male sterility. J.Exp.Bot. *67*, 5557–5569. https://doi.org/10.1093/jxb/erw324.
22. Geigenberger, P. (2011). Regulation of starch biosynthesis in response to a fluctuating environment. Plant Physiol. *155*, 1566–1577. https://doi.org/10.1104/pp.110.170399.
23. Geigenberger, P., Stitt, M., and Fernie, A.R. (2004). Metabolic control analysis and regulation of the conversion of sucrose to starch in growing potato tubers. PlantCellEnviron. *27*, 655–673. https://doi.org/10.1111/j.1365-3040.2004.01183.x.
24. Dickinson, D.B. (1965). Germination of lilypollen: respiration and tubegrowth. Science *150*, 1818–1819. https://doi.org/10.1126/science.150.3705.1818.
25. Dickinson, D.B. (1966). Inhibition of pollenrespiration by oligomycin. Nature *210*, 1362–1363. https://doi.org/10.1038/2101362a0.
26. Dickinson, D.B. (1968). Rapid starch synthesis associated with increased respiration in germinating lily pollen. Plant Physiol. *43*, 1–8. https://doi.org/10.1104/pp.43.1.1.
27. Franckowiak, J.D., and Lundqvist, U. (2012). Descriptions of barleygeneticstocks for 2012. Barley Genet.Newsl. *42*, 36–173 https://wheat.pw.usda.gov/ggpages/bgn/42/index.html.
28. Druka, A., Franckowiak, J., Lundqvist, U., Bonar, N., Alexander, J., Houston, K., Radovic, S., Shahinnia, F., Vendramin, V., Morgante, M., et al. (2011). Genetic dissection of barley morphology and development. Plant Physiol. *155*, 617–627. https://doi.org/10.1104/pp.110.166249.

29. Waddington, S.R., Cartwright, P.M., and Wall, P.C. (1983). A quantitativescale of spikeinitial and pistildevelopment in barley and wheat. Ann.Bot. *51*, 119–130.

30. Matsui, T., Omasa, K., and Horie, T. (2000). Rapid swelling of pollengrains in the dehiscinganther of two-rowed barley (*Hordeum distichum* L. emend. Lam.). Ann.Bot. *85*, 345–350. https://doi.org/10.1006/anbo.1999.1051.

31. Rehman, S., Rha, E.S., Ashraf, M., Lee, K.J., Yun, S.J., Kwak, Y.G., Yoo, N.H., and Kim, J.K. (2004). Does barley (*Hordeum vulgare* L.) pollen swell in fractions of a second? Plant Sci. *167*, 137–142. https://doi.org/10.1016/j.plantsci.2004.03.013.

32. Mashiguchi, K., Tanaka, K., Sakai, T., Sugawara, S., Kawaide, H., Natsume, M., Hanada, A., Yaeno, T., Shirasu, K., Yao, H., et al. (2011). The main auxin biosynthesis pathway in *Arabidopsis*. Proc.Natl.Acad.Sci. USA *108*, 18512–18517. https://doi.org/10.1073/pnas.1108434108.

33. Won, C., Shen, X., Mashiguchi, K., Zheng, Z., Dai, X., Cheng, Y., Kasahara, H., Kamiya, Y., Chory, J., and Zhao, Y. (2011). Conversion of tryptophan to indole-3-acetic acid by TRYPTOPHAN AMINOTRANSFERASES OF *ARABIDOPSIS* and YUCCAs in *Arabidopsis*. Proc.Natl.Acad.Sci. USA *108*, 18518–18523. https://doi.org/10.1073/pnas.1108436108.

34. Sieber, M.H., and Spradling, A.C. (2017). The role of metabolic states in development and disease. Curr.Opin.Genet.Dev. *45*, 58–68. https://doi.org/10.1016/j.gde.2017.03.002.

35. Tennessen, J.M., Baker, K.D., Lam, G., Evans, J., and Thummel, C.S. (2011). The *Drosophila* estrogen-related receptor directs a metabolic switch that supports developmental growth. Cell Metab. *13*, 139–148. https://doi.org/10.1016/j.cmet.2011.01.005.

36. Verbist, K.C., Guy, C.S., Milasta, S., Liedmann, S., Kamiński, M.M., Wang, R., and Green, D.R. (2016). Metabolic maintenance of cell asymmetry following division in activated T lymphocytes. Nature *532*, 389–393. https://doi.org/10.1038/nature17442.

37. Fu, L., Liu, Y., Qin, G., Wu, P., Zi, H., Xu, Z., Zhao, X., Wang, Y., Li, Y., Yang, S., et al. (2021). The TOR-EIN2 axis mediates nuclear signalling to modulate plant growth. Nature *591*, 288–292. https://doi.org/10.1038/s41586-021-03310-y.

38. Li, S., Tian, Y., Wu, K., Ye, Y., Yu, J., Zhang, J., Liu, Q., Hu, M., Li, H., Tong, Y., et al. (2018). Modulating plant growth-metabolism coordination for sustainable agriculture. Nature *560*, 595–600. https://doi.org/10.1038/s41586-018-0415-5.

39. Rolletschek, H., Weschke, W., Weber, H., Wobus, U., and Borisjuk, L. (2004). Energy state and its control on seed development: starch accumulation is associated with high ATP and steep oxygen gradients within barley grains. J.Exp.Bot. *55*, 1351–1359. https://doi.org/10.1093/jxb/erh130.

40. Bernardi, J., Battaglia, R., Bagnaresi, P., Lucini, L., and Marocco, A. (2019). Transcriptomic and metabolomic analysis of ZmYUC1 mutant reveals the role of auxin during early endosperm formation in maize. Plant Sci. *281*, 133–145. https://doi.org/10.1016/j.plantsci.2019.01.027.

41. McAdam, E.L., Meitzel, T., Quittenden, L.J., Davidson, S.E., Dalmais, M., Bendahmane, A.I., Thompson, R., Smith, J.J., Nichols, D.S., Urquhart, S., et al. (2017). Evidence that auxin is required for normal seed size and starch synthesis in pea. New Phytol. *216*, 193–204. https://doi.org/10.1111/nph.14690.

42. Commoner, B., and Thimann, K.V. (1941). On the relation between growth and respiration in the *Avena*coleoptile. J.Gen.Physiol. *24*, 279–296. https://doi.org/10.1085/jgp.24.3.279.

43. Leonova, L.A., Gamburg, K.Z., Vojnikov, V.K., and Varakina, N.N. (1985). Promotion of respiration by auxin in the induction of cell division in suspension culture. J.Plant Growth Regul. *4*, 169–176. https://doi.org/10.1007/BF02266954.

44. Batista-Silva, W., Medeiros, D.B., Rodrigues-Salvador, A., Daloso, D.M., Omena-Garcia, R.P., Oliveira, F.S., Pino, L.E., Peres, L.E.P., Nunes-Nesi, A., Fernie, A.R., et al. (2019). Modulation of auxin signalling through DIAGETROPICA and ENTIRE differentially affects tomato plant growth via changes in photosynthetic and mitochondrial metabolism. Plant Cell Environ. *42*, 448–465. https://doi.org/10.1111/pce.13413.

45. Mair, A., Pedrotti, L., Wurzinger, B., Anrather, D., Simeunovic, A., Weiste, C., Valerio, C., Dietrich, K., Kirchler, T., Nägele, T., et al. (2015). SnRK1-triggered switch of bZIP63 dimerization mediates the low-energy response in plants. eLife *4*, https://doi.org/10.7554/eLife.05828.

46. Nukarinen, E., Nägele, T., Pedrotti, L., Wurzinger, B., Mair, A., Landgraf, R., Börnke, F., Hanson, J., Teige, M., Baena-Gonzalez, E., et al. (2016). Quantitative phosphoproteomics reveals the role of the AMPK plant ortholog SnRK1 as a metabolic master regulator under energy deprivation. Sci.Rep. *6*, 31697. https://doi.org/10.1038/srep31697.

47. Krouk, G., Ruffel, S., Gutiérrez, R.A., Gojon, A., Crawford, N.M., Coruzzi, G.M., and Lacombe, B. (2011). A framework integrating plant growth with hormones and nutrients. Trends Plant Sci. *16*, 178–182. https://doi.org/10.1016/j.tplants.2011.02.004.

48. Zhang, Y., Shewry, P.R., Jones, H., Barcelo, P., Lazzeri, P.A., and Halford, N.G. (2001). Expression of antisense SnRK1 protein kinase sequence causes abnormal pollen development and male sterility in transgenic barley. Plant J. *28*, 431–441. https://doi.org/10.1046/j.1365-313x.2001.01167.x.

49. Kuang, A., and Musgrave, M.E. (1996). Dynamics of vegetative cytoplasm during generative cell formation and pollen maturation in *Arabidopsis thaliana*. Protoplasma *194*, 81–90. https://doi.org/10.1007/BF01273170.

50. Brumos, J., Robles, L.M., Yun, J., Vu, T.C., Jackson, S., Alonso, J.M., and Stepanova, A.N. (2018). Local auxinbiosynthesisis a keyregulator of plantdevelopment. Dev. Cell *47*, 306–318.e5. https://doi.org/10.1016/j.devcel.2018.09.022.

51. Cecchetti, V., Celebrin, D., Napoli, N., Ghelli, R., Brunetti, P., Costantino, P., and Cardarelli, M. (2017). An auxin maximum in the middle layer controls stamen development and pollen maturation in *Arabidopsis*. New Phytol. *213*, 1194–1207. https://doi.org/10.1111/nph.14207.

52. Franckowiak, J.D., and Hockett, E.A. (1988). Identification of three new loci which control male sterility of barley. Barley Genet.Newsl. *18*, 11–13.

53. Hockett, E.A. (1984). Identification of three new loci which control male sterility of barley. Barley Genet.Newsl. *14*, 70–75.

54. Wilson, S.M., and Bacic, A. (2012). Preparation of plant cells for transmission electron microscopy to optimize immunogold labeling of carbohydrate and protein epitopes. Nat.Protoc. *7*, 1716–1727. https://doi.org/10.1038/nprot.2012.096.

55. Peterson, R., Slovin, J.P., and Chen, C. (2010). A simplified method for differential staining of aborted and non-aborted pollen grains. Int.J.Plant Biol. *1*, e13.

56. Alexander, M.P. (1969). Differential staining of aborted and nonaborted pollen. Stain Technol. *44*, 117–122. https://doi.org/10.3109/10520296909063335.

57. Aloni, B., Peet, M., Pharr, M., and Karni, L. (2001). The effect of high temperature and high atmospheric CO_2 on carbohydrate changes in bell pepper (*Capsicum annuum*) pollen in relation to its germination. Physiol. Plant *112*, 505–512. https://doi.org/10.1034/j.1399-3054.2001.1120407.x.

58. Liu, R.-S., Qiu, Y.-L., Wei, D.-M., Liu, H.-H., Zhu, X.-Y., Tian, H.-Q., and Teixeira da Silva, J.A.T. (2011). Distribution of starch and neutral lipids in the developing anthers of *Ipomoea cairica*. Ann.Bot.Fenn. *48*, 256–262.

59. Wang, S., Zhang, Y., Fang, Z., Zhang, Y., Song, Q., Hou, Z., Sun, K., Song, Y., Li, Y., Ma, D., et al. (2019). Cytological and proteomicanalysis of wheatpollenabortioninduced by chemicalhybridizationagent. Int.J.Mol.Sci. *20*, https://doi.org/10.3390/ijms20071615.

60. Gomori, G. (1952). Microscopic Histochemistry. Principles and Practice (The University of Chicago Press).

61. Mascher, M., Gundlach, H., Himmelbach, A., Beier, S., Twardziok, S.O., Wicker, T., Radchuk, V., Dockter, C., Hedley, P.E., Russell, J., et al. (2017). A chromosome conformation capture ordered sequence of the

barley genome. Nature *544*, 427–433. https://doi.org/10.1038/nature22043.

62. Monat, C., Padmarasu, S., Lux, T., Wicker, T., Gundlach, H., Himmelbach, A., Ens, J., Li, C., Muehlbauer, G.J., Schulman, A.H., et al. (2019). TRITEX: chromosome-scale sequence assembly of Triticeae genomes with open-source tools. Genome Biol. *20*, 284. https://doi.org/10.1186/s13059-019-1899-5.

63. Gol, L., Haraldsson, E.B., and von Korff, M. (2021). Ppd-H1 integrates drought stress signals to control spike development and flowering time in barley. J.Exp.Bot. *72*, 122–136. https://doi.org/10.1093/jxb/eraa261.

64. Lawrenson, T., Shorinola, O., Stacey, N., Li, C., Østergaard, L., Patron, N., Uauy, C., and Harwood, W. (2015). Induction of targeted, heritable mutations in barley and *Brassica oleracea* using RNA-guided Cas9 nuclease. Genome Biol. *16*, 258. https://doi.org/10.1186/s13059-015-0826-7.

65. Schindelin, J., Arganda-Carreras, I., Frise, E., Kaynig, V., Longair, M., Pietzsch, T., Preibisch, S., Rueden, C., Saalfeld, S., Schmid, B., et al. (2012). Fiji: an open-source platform for biological-image analysis. Nat. Methods *9*, 676–682. https://doi.org/10.1038/nmeth.2019.

66. Bolger, A.M., Lohse, M., and Usadel, B. (2014). Trimmomatic: a flexible trimmer for Illumina sequence data. Bioinformatics *30*, 2114–2120. https://doi.org/10.1093/bioinformatics/btu170.

67. Langmead, B., and Salzberg, S.L. (2012). Fast gapped-read alignment with Bowtie 2. Nat. Methods *9*, 357–359. https://doi.org/10.1038/nmeth.1923.

68. Li, H. (2011). A statistical framework for SNP calling, mutation discovery, association mapping and population genetical parameter estimation from sequencing data. Bioinformatics *27*, 2987–2993. https://doi.org/10.1093/bioinformatics/btr509.

69. McKenna, A., Hanna, M., Banks, E., Sivachenko, A., Cibulskis, K., Kernytsky, A., Garimella, K., Altshuler, D., Gabriel, S., Daly, M., and DePristo, M.A. (2010). The Genome Analysis Toolkit: a MapReduce framework for analyzing next-generation DNA sequencing data. Genome Res. *20*, 1297–1303. https://doi.org/10.1101/gr.107524.110.

70. Danecek, P., Auton, A., Abecasis, G., Albers, C.A., Banks, E., DePristo, M.A., Handsaker, R.E., Lunter, G., Marth, G.T., Sherry, S.T., et al. (2011). The variant call format and VCFtools. Bioinformatics *27*, 2156–2158. https://doi.org/10.1093/bioinformatics/btr330.

71. Kumar, S., Stecher, G., Li, M., Knyaz, C., and Tamura, K. (2018). MEGA X: molecular evolutionarygeneticsanalysis across computingplatforms. Mol.Biol.Evol. *35*, 1547–1549. https://doi.org/10.1093/molbev/msy096.

72. Ronquist, F., Teslenko, M., van der Mark, P., Ayres, D.L., Darling, A., Höhna, S., Larget, B., Liu, L., Suchard, M.A., and Huelsenbeck, J.P. (2012). MrBayes 3.2: efficient Bayesian phylogenetic inference and model choice across a large model space. Syst.Biol. *61*, 539–542. https://doi.org/10.1093/sysbio/sys029.

73. Ruijter, J.M., Ramakers, C., Hoogaars, W.M., Karlen, Y., Bakker, O., van den Hoff, M.J., and Moorman, A.F. (2009). Amplification efficiency: linking baseline and bias in the analysis of quantitative PCR data. Nucleic Acids Res. *37*, e45. https://doi.org/10.1093/nar/gkp045.

74. Patro, R., Duggal, G., Love, M.I., Irizarry, R.A., and Kingsford, C. (2017). Salmon provides fast and bias-aware quantification of transcript expression. Nat. Methods *14*, 417–419. https://doi.org/10.1038/nmeth.4197.

75. Mejía-Guerra, M.K., and Buckler, E.S. (2019). A k-mer grammar analysis to uncover maize regulatory architecture. BMC Plant Biol. *19*, 103. https://doi.org/10.1186/s12870-019-1693-2.

76. Mori, T., Kuroiwa, H., Higashiyama, T., and Kuroiwa, T. (2006). GENERATIVE CELL SPECIFIC 1 is essential for angiosperm fertilization. Nat. Cell Biol. *8*, 64–71. https://doi.org/10.1038/ncb1345.

77. Liu, L., Zheng, C., Kuang, B., Wei, L., Yan, L., and Wang, T. (2016). Receptor-likekinase RUPO interacts with potassiumtransporters to regulatepollentubegrowth and integrity in rice. PLOS Genet. *12*, e1006085. https://doi.org/10.1371/journal.pgen.1006085.

78. Micali, C.O., Neumann, U., Grunewald, D., Panstruga, R., and O'Connell, R. (2011). Biogenesis of a specialized plant-fungal interface during host cell internalization of *Golovinomyces orontii* haustoria. Cell.Microbiol. *13*, 210–226. https://doi.org/10.1111/j.1462-5822.2010.01530.x.

79. Phillips, D., Jenkins, G., Macaulay, M., Nibau, C., Wnetrzak, J., Fallding, D., Colas, I., Oakey, H., Waugh, R., and Ramsay, L. (2015). The effect of temperature on the male and female recombination landscape of barley. New Phytol. *208*, 421–429. https://doi.org/10.1111/nph.13548.

80. Edgar, R.C. (2004). MUSCLE: multiple sequence alignment with high accuracy and high throughput. Nucleic Acids Res. *32*, 1792–1797. https://doi.org/10.1093/nar/gkh340.

81. Jöst, M., Hensel, G., Kappel, C., Druka, A., Sicard, A., Hohmann, U., Beier, S., Himmelbach, A., Waugh, R., Kumlehn, J., et al. (2016). The INDETERMINATE DOMAIN protein BROAD LEAF1 limitsbarleyleafwidth by restrictinglateralproliferation. Curr.Biol. *26*, 903–909. https://doi.org/10.1016/j.cub.2016.01.047.

82. Hensel, G., Kastner, C., Oleszczuk, S., Riechen, J., and Kumlehn, J. (2009). Agrobacterium-mediated gene transfer to cereal crop plants: current protocols for barley, wheat, triticale, and maize. Int.J. Plant Genomics *2009*, 835608. https://doi.org/10.1155/2009/835608.

83. Novák, O., Hényková, E., Sairanen, I., Kowalczyk, M., Pospíšil, T., and Ljung, K. (2012). Tissue-specific profiling of the *Arabidopsis thaliana* auxin metabolome. Plant J. *72*, 523–536. https://doi.org/10.1111/j.1365-313X.2012.05085.x.

84. Oñate-Sánchez, L., and Vicente-Carbajosa, J. (2008). DNA-free RNA isolation protocols for *Arabidopsis thaliana*, including seeds and siliques. BMC Res. Notes *1*, 93. https://doi.org/10.1186/1756-0500-1-93.

85. Jackson, D. (1992). In situ hybridization in plants. In Molecular Plant Pathology, *1*, S.J. Gurr, M.J. McPherson, and D.J. Bowles, eds. (IRL Press), pp. 163–174.

86. Bortiri, E., Chuck, G., Vollbrecht, E., Rocheford, T., Martienssen, R., and Hake, S. (2006). *ramosa2* encodes a LATERAL ORGAN BOUNDARY domain protein that determines the fate of stem cells in branch meristems of maize. Plant Cell *18*, 574–585.

87. Chauvin, A., Caldelari, D., Wolfender, J.L., and Farmer, E.E. (2013). Four 13-lipoxygenases contribute to rapid jasmonate synthesis in wounded *Arabidopsis thaliana* leaves: a role for lipoxygenase 6 in responses to long-distance wound signals. New Phytol. *197*, 566–575. https://doi.org/10.1111/nph.12029.

88. Robinson, M.D., McCarthy, D.J., and Smyth, G.K. (2010). edgeR: a Bioconductor package for differential expression analysis of digital gene expression data. Bioinformatics *26*, 139–140. https://doi.org/10.1093/bioinformatics/btp616.

89. Ritchie, M.E., Phipson, B., Wu, D., Hu, Y., Law, C.W., Shi, W., and Smyth, G.K. (2015). limma powers differential expression analyses for RNA-sequencing and microarray studies. Nucleic Acids Res. *43*, e47. https://doi.org/10.1093/nar/gkv007.

90. Zhong, J., van Esse, G.W., Bi, X., Lan, T., Walla, A., Sang, Q., Franzen, R., and von Korff, M. (2021). INTERMEDIUM-M encodes an HvAP2L-H5 ortholog and is required for inflorescence indeterminacy and spikelet determinacy in barley. Proc.Natl.Acad.Sci. USA *118*, https://doi.org/10.1073/pnas.2011779118.

91. Alexa, A., Rahnenführer, J., and Lengauer, T. (2006). Improved scoring of functional groups from gene expression data by decorrelating GO graph structure. Bioinformatics *22*, 1600–1607. https://doi.org/10.1093/bioinformatics/btl140.

92. Hedhly, A., Vogler, H., Schmid, M.W., Pazmino, D., Gagliardini, V., Santelia, D., and Grossniklaus, U. (2016). Starch turnover and metabolism during flower and earlyembryodevelopment. Plant Physiol. *172*, 2388–2402. https://doi.org/10.1104/pp.16.00916.

93. Schwacke, R., Schneider, A., van der Graaff, E., Fischer, K., Catoni, E., Desimone, M., Frommer, W.B., Flügge, U.I., and Kunze, R. (2003). ARAMEMNON, a novel database for *Arabidopsis* integral membrane proteins. Plant Physiol. *131*, 16–26. https://doi.org/10.1104/pp.011577.

94. Elbourne, L.D., Tetu, S.G., Hassan, K.A., and Paulsen, I.T. (2017). TransportDB 2.0: a database for exploring membrane transporters in sequenced genomes from all domains of life. Nucleic Acids Res. *45*, D320–D324. https://doi.org/10.1093/nar/gkw1068.

95. Michard, E., Simon, A.A., Tavares, B., Wudick, M.M., and Feijó, J.A. (2017). Signaling with ions: thekeystone for apicalcellgrowth and morphogenesis in pollentubes. Plant Physiol. *173*, 91–111. https://doi.org/10.1104/pp.16.01561.

96. Galli, M., Khakhar, A., Lu, Z., Chen, Z., Sen, S., Joshi, T., Nemhauser, J.L., Schmitz, R.J., and Gallavotti, A. (2018). The DNA binding landscape of the maize AUXIN RESPONSE FACTOR family. Nat.Commun. *9*, 4526. https://doi.org/10.1038/s41467-018-06977-6.

97. Tu, X., Mejía-Guerra, M.K., Valdes Franco, J.A., Tzeng, D., Chu, P.Y., Shen, W., Wei, Y., Dai, X., Li, P., Buckler, E.S., and Zhong, S. (2020). Reconstructing the maize leaf regulatory network using ChIP-seq data of 104 transcription factors. Nat.Commun. *11*, 5089. https://doi.org/10.1038/s41467-020-18832-8.

98. Lisec, J., Schauer, N., Kopka, J., Willmitzer, L., and Fernie, A.R. (2006). Gas chromatography mass spectrometry-based metabolite profiling in plants. Nat.Protoc. *1*, 387–396.

99. Kopka, J., Schauer, N., Krueger, S., Birkemeyer, C., Usadel, B., Bergmüller, E., Dörmann, P., Weckwerth, W., Gibon, Y., Stitt, M., et al. (2005). GMD@CSB. DB: the Golm metabolome database. Bioinformatics *21*, 1635–1638.

100. Rosado-Souza, L., David, L.C., Drapal, M., Fraser, P.D., Hofmann, J., Klemens, P.A.W., Ludewig, F., Neuhaus, H.E., Obata, T., Perez-Fons, L., et al. (2019). Cassava metabolomics and starch quality. Curr.Protoc.PlantBiol. *4*, e20102.

Please cite this article in press as: Amanda et al., Auxin boosts energy generation pathways to fuel pollen maturation in barley, Current Biology (2022), https://doi.org/10.1016/j.cub.2022.02.073

STAR★METHODS

KEY RESOURCES TABLE

REAGENT or RESOURCE	SOURCE	IDENTIFIER
Chemicals, peptides, and recombinant proteins		
Perfluorperhydrophenanthren	Sigma-Aldrich	56919
Deposited data		
Raw RNAseq data: Bowman and *msg38*	This paper	ENA: PRJEB47154
Raw RNAseq data: Several cultivars	James Hutton Institute, European Nucleotide Archive	ENA: PRJEB3130
Barley reference genome V1 (Transcripts of high-confidence and low-confidence gene sets)	Mascher et al.[61]	https://doi.org/10.5447/IPK/2016/40; https://doi.org/10.5447/IPK/2016/48
Barley reference genome V2	Mascher et al.[62]	https://doi.org/10.5447/ipk/2019/8
Plant YUCCA protein sequences	ENSEMBLPlants, NCBI, etc.	See Data S1B
Experimental models: Organisms/strains		
Barley: cultivar Bowman	GRIN-USDA	PI 483237 https://npgsweb.ars-grin.gov/gringlobal/search
Barley: *msg38* (Bowman introgression)	J.D. Franckowiak[28]; GRIN-USDA	GSHO 2304 https://npgsweb.ars-grin.gov/gringlobal/search
Barley: cultivar Golden Promise Fast (*Ppd-H1*)	M. von Korff[63]	N/A
Barley: *msg38-2*	This paper	*msg38-2*
Barley: *msg38-3*	This paper	*msg38-3*
Barley: *yuc2* (five-allele mutant series)	This paper	*yuc2-1* to *yuc2-5*
Barley: *MSG38pro*-MSG38-Citrine	This paper	N/A
Oligonucleotides		
See Data S1A and S1N	This paper	N/A
Recombinant DNA		
Golden Gate plasmid for gene editing: Promoter, U6 (*Triticum aestivum*, pICSL9003)	Lawrenson et al.[64]	AddGene 68262
Golden Gate plasmid for gene editing: Level 1, position 3 acceptor (pICH47751)	Lawrenson et al.[64]	AddGene 48002
Golden Gate plasmid for gene editing: Level 1, position 4 acceptor (pICH47761)	Lawrenson et al.[64]	AddGene 48003
Golden Gate plasmid for gene editing: Barley plant selection cassette (pICSL11059)	Lawrenson et al.[64]	AddGene 68263
Golden Gate plasmid for gene editing: Barley Cas9 cassette (pICSL11056)	Lawrenson et al.[64]	AddGene 68258
Golden Gate plasmid for gene editing: Position 4 end linker (pICH50900)	Lawrenson et al.[64]	AddGene 48047
Golden Gate for gene editing: Binary Vector Backbone; Level M acceptor (pAGM8031)	Lawrenson et al.[64]	AddGene 48037
Gene editing: Cas9_sgRNA1_sgRNA2_MSG38/HvYUC4	This paper	pMP115
Gene editing: Cas9_sgRNA1_sgRNA2_HvYUC2	This paper	pMP164
Gateway-based fluorescent reporter vector for barley: pDEST_2X35S-Hygro_34GW	This paper	pMP154
MSG38 fluorescent reporter: HvMSG38_genomic-5.3kb-Citrine	This paper	pMP157

(*Continued on next page*)

Please cite this article in press as: Amanda et al., Auxin boosts energy generation pathways to fuel pollen maturation in barley, Current Biology (2022), https://doi.org/10.1016/j.cub.2022.02.073

Continued

REAGENT or RESOURCE	SOURCE	IDENTIFIER
Software and algorithms		
Zen 2.3 blue edition	Carl Zeiss Microscopy GmbH	www.zeiss.com/microscopy/int/products/microscope-software/zen.html
Fiji (ImageJ v1.52n)	Schindelin et al.[65]	https://imagej.net/software/fiji/downloads
Leica Application Suite X v3.5.7	Leica Microsystems	www.leica-microsystems.com/
FastQC v0.11.5	Bioinformatics Group, Babraham Institute	https://www.bioinformatics.babraham.ac.uk/projects/fastqc/
Trimmomatic v0.35	Bolger et al.[66]	http://www.usadellab.org/cms/?page=trimmomatic
Bowtie 2	Langmead and Salzberg[67]	http://bowtie-bio.sourceforge.net/bowtie2/index.shtml
SAMtools v1.3.1	H. Li[68]	http://www.htslib.org/
Picard v1.141	Broad Institute	http://broadinstitute.github.io/picard
GATK v3.5-0	McKenna et al.[69]	https://gatk.broadinstitute.org/
VCFtools v0.1.13	Danecek et al.[70]	https://vcftools.github.io/
R v4.0.4	The R Foundation	www.r-project.org/
RStudio 1.4.1106	RStudio Public Benefit Corporation	https://www.rstudio.com/
MEGA-X v10.1.7	Kumar et al.[71]	www.megasoftware.net
MrBayes v3.2.7	Ronquist et al.[72]	http://nbisweden.github.io/MrBayes/
FigTree v1.4.4	A. Rambaut	https://github.com/rambaut/figtree/releases
LinRegPCR 2020.0	Ruijter et al.[73]	https://medischebiologie.nl/files/
Salmon v1.4	Patro et al.[74]	https://salmon.readthedocs.io/en/latest/salmon.html
k-mer grammar for machine learning model	Mejia et al.[75]	https://bitbucket.org/bucklerlab/k-mer_grammar/
ChromaTOF v1.00 (Pegasus driver 1.61)	Laboratory Equipment Company (LECO)	https://www.leco.com/product/chromatof-software
Xcalibur Software v4.3	Thermo Scientific	Catalog# OPTON-30965

RESOURCE AVAILABILITY

Lead contact

Further information and requests for resources and reagents should be directed to and will be fulfilled by the lead contact, Ivan F. Acosta (acosta@mpipz.mpg.de).

Materials availability

Plasmids and seeds are available from the lead contact under a transfer agreement with Max Planck Institute for Plant Breeding Research.

Data and code availability

- Raw RNAseq data have been deposited at the European Nucleotide Archive (ENA) and are publicly available as of the date of publication. The accession number is listed in the key resources table. All other data (quantifications and microscopy images) is available in the main text, the supplementary materials or from the lead contact upon request.
- This paper does not report original code.
- Any additional information required to reanalyze the data reported in this paper is available from the lead contact upon request.

EXPERIMENTAL MODEL AND SUBJECT DETAILS

Plant material

Barley (*Hordeum vulgare* subsp. *vulgare*) cultivar Bowman and segregating populations of *msg38* seeds were obtained from the GRIN-USDA seed bank. We generated transgenic plants via stable transformation in ‘‘Golden Promise Fast’’, the *Ppd-H1*

Please cite this article in press as: Amanda et al., Auxin boosts energy generation pathways to fuel pollen maturation in barley, Current Biology (2022), https://doi.org/10.1016/j.cub.2022.02.073

introgression line of the transformable barley cultivar Golden Promise, which was kindly provided by Maria von Korff. The wild-type *Ppd-H1* allele in this line confers early flowering.[63] Transgenic lines generated in this background include gene-edited mutant alleles *msg38-2*, *msg38-3* and *yuc2-1* to *yuc2-5*, as well as *MSG38pro*-MSG38-Citrine.

Plant genotyping

The original *msg38* mutant was found spontaneously in the cultivar Ingrid.[27,52,53] The mutation has been backcrossed at least six times into the cultivar Bowman[28] and throughout this work we used mainly this introgression line, simply referred to as *msg38*. Due to its complete male sterility, we currently maintain the *msg38* mutant allele in heterozygous *msg38*/+ individuals. Progenies of these plants are screened with PCR genotyping with primers 165 and 166 (Data S1A) to identify homozygous *msg38* mutants at seedling stage. *msg38-2* and *msg38-3* mutant alleles are genotyped with primers 165 and 225 (Data S1A).

Growth conditions

Seeds were sown in 96-well trays filled with a 1:1 mix of soil ED 73 Einheitserde® (Einheitserdewerke Werkverband e.V., Sinntal-Altengronau, Germany) to BVB Substrates (1:1 vermiculite to coconut fiber). Between one or two weeks later, seedlings were transplanted to 1-Liter pots containing the same substrate. Plants grew in greenhouses under long-day controlled conditions (16h light, 22°C; 8h dark, 18 °C) and reached anthesis ~7–8 weeks-after-planting in Bowman and ~6–7 weeks-after-planting in Golden Promise Fast.

METHOD DETAILS

Stamen and pistil imaging

Reproductive organs were dissected out of florets with fine forceps under a common stereomicroscope, visualized with a Discovery.V12 stereomicroscope and imaged with a Stemi 503 color camera and Zen 2.3 blue edition software (Carl Zeiss).

Light microscopy

A Carl Zeiss Axio Scope.A1 was used for sample examination with light microscopy, and images were acquired with an Axiocam 512 color camera and Zen 2.3 blue edition software (Carl Zeiss).

Anther histology

Florets were fixed in freshly prepared 1x PBS (pH 7.4) containing 1% (v/v) glutaraldehyde, 4% (v/v) paraformaldehyde and 0.03% Triton X-100. Samples were processed for embedding in LR White medium grade resin (London Resin Company Ltd) as described.[54] Resin blocks with samples were trimmed (TM 60 block trimmer, Reichert-Jung) and transverse semi-thin sections (1 μm) were cut with a diamond knife (DiATOME histo 6,0 mm) clamped to a microtome (UltraCut U1, Reichert-Jung). Sections were mounted in epoxy-coated, 12-welled diagnostic microscope slides (Menzel) and stained with a Toluidine Blue + Borax solution (each 1% w/v). After a brief rinse with running water, slides were stored dry for later imaging with light microscopy.

Pollen viability assay with Alexander's staining

Florets at W9.75 (anther opening stage) were fixed in Carnoy's solution (6:3:1 :: ethanol: chloroform: glacial acetic acid) and stained with a simplification of Alexander's method[55] but with addition of chloral hydrate as described in the original protocol[56] and the following modifications. Fixed samples were moved to staining solution in 1.5-ml tubes and incubated at 100 °C for 1.5 h. The staining solution was replaced twice with mounting solution (70 % glycerol in 10 mM Tris-HCL, pH 8.0) and the samples were cleared on a rotary wheel overnight before pollen imaging.

Detection of pollen starch with light microscopy

Anthers at W9.75 were halved transversally and immersed in I_2/KI solution (0.3 g/1.5 g per 100 ml H_2O) in 1.5-ml tubes, as described.[57] After staining, anthers were vortexed and spun briefly to collect pollen grains for imaging.

Basic fuchsin in the periodic acid-Schiff reaction was used to visualize starch granules in more detail in 1-μm semi-thin sections of florets ("Anther histology" above). The first part of the staining was as described.[58] In brief, the sections were incubated with 0.5% (w/v) periodic acid solution in 0.3% (w/v) nitric acid for 10 mins at room temperature. Slides were washed with running distilled water for 1–2 mins and incubated with Schiff's reagent (0.5% w/v basic fuchsin in water) for 30 mins. Subsequent destaining with 5% (w/v) sodium metabisulfite caused the insoluble polysaccharide to turn purple or pink.[59]

Detection of potassium salt crystals in pollen

We prepared Macallum's solution as described,[60] under a fume hood: 5 g cobalt nitrate were dissolved in a mix of 10 ml water and 2.5 ml acetic acid to make solution A, and 15 sodium nitrate were dissolved in 25 ml water to make solution B. Both solutions were mixed and shaken for a few minutes to allow evaporation of generated nitrous fumes. The solution can be stored for maximum of two weeks. Transversally halved anthers at W9.75 were placed in Macallum's staining solution in 1.5-ml tubes for 30 mins. The solution was replaced with ice-cold water for 5 mins. Pollen grains collected after a brief vortex and centrifugation were mounted in a 1:1 solution of 50% glycerol: 2.5% ammonium sulfide for imaging.

Please cite this article in press as: Amanda et al., Auxin boosts energy generation pathways to fuel pollen maturation in barley, Current Biology (2022), https://doi.org/10.1016/j.cub.2022.02.073

Area of fresh pollen without mounting medium

For all stages before anther opening, anthers were opened carefully with fine forceps under a stereomicroscope to collect pollen grains, which were spread on dry glass slides without cover slip nor liquid mounting medium for imaging. Pollen areas were measured with Fiji[65] from images converted to grayscale 8-bits. Since pollen grains appear dehydrated at most stages, they were measured only when the folded external wall was facing upwards, as in Figure 1F. Fiji's functions *threshold*, *watershed*, *paintbrush* and *analyze particles* (varying the parameter *size*) were used to select, separate, clean and measure pollen grains, respectively. We used the same method to quantify the area of fixed pollen grains treated with Alexander's stain (see above) for the plots in Figures 2B, 2C, and S5B.

Scanning electron microscopy

Pollen from W9.75 anthers was mounted on pin stubs using double-sided adhesive and conductive tabs. Samples were then sputter-coated with gold and imaged with a Zeiss Supra 40VP scanning electron microscope (Carl Zeiss).

Pollen germination assay

We followed two published protocols[76,77] with some modifications. Pistils approaching stage W9.75 were manually pollinated with Bowman or *msg38* pollen. Nineteen hours after pollination spikelets were fixed in ethanol: acetic acid (3:1) for 30 mins, rinsed with water and placed in 1M NaOH for 30 mins at 55°C, before staining with 0.1% (w/v) aniline blue in 0.1 M K_2HPO_4 (pH 8.5) at room temperature for 1 hour in the dark. Samples were mounted in perfluorperhydrophenanthren (Sigma-Aldrich/Merck) and examined with an SP8 laser confocal scanning microscope (Leica Microsystems), a 405 nm laser beam line and a HyD detector (emitted fluorescence captured between 447–471 nm).

Pollen nuclei visualization with DAPI staining

Transversally-halved anthers were placed in 1.5-ml tubes with DAPI staining solution (1μg/ml DAPI, 1% Triton-X in 1x PBS, pH 7.4) and incubated for 1 hour at room temperature. Anthers were dissected with fine forceps to extract pollen grains on a microscope slide containing 70 % glycerol in 10 mM Tris-HCl, pH 8.0. Pollen was examined with the SP8 laser confocal scanning microscope (405 nm laser beam line and HyD detector; emitted fluorescence captured between 445–470nm).

Transmission electron microscopy

Stamens were high-pressure frozen, freeze substituted and imaged as described[78] with minor modifications. The last steps of the freeze substitution program were: 12 h at -20°C, transition to 4°C at 12°C/h (2 h) and 3.5 h at 4°C. Sections were contrasted with 0.1 % potassium permanganate in 0.1 N H_2SO_4 for 1 min, before staining with uranyl acetate and lead citrate. To improve visualization, the contrast of all images within a given panel was changed with the same settings in Adobe Photoshop 21.2.11.

MSG38 gene identification

Previous high-throughput genotyping of the *msg38*-Bowman introgression lines identified two regions in chromosomes 2 and 3 potentially carrying the *MSG38* locus.[28] We confirmed linkage of the mutation with the region in the lower arm of chromosome 3. Further genotyping of *msg38* segregating populations with public and newly identified DNA markers, narrowed down the locus to a 0.8 cM interval (Figure 3A; Data S1A).

Concurrently, we performed RNAseq of *msg38* and wild-type Bowman stamens at stages W9.25 and W9.35 to detect gene variants within that interval. Total RNA was extracted (see below) from four biological replicates per genotype per stage, each containing the stamens of 7 to 18 florets. Ribosomal RNA depletion, library preparation and RNA sequencing of 20 million 100-bp single reads were performed at the Max Planck-GenomeCentre Cologne.

Sequencing data was quality-checked with FastQC v0.11.5. Reads were trimmed with Trimmomatic v0.35[66] and the following parameters: ILLUMINACLIP: Trimmomatic-0.35/adapters/TruSeq3-SE.fa:2:30:10 LEADING: 3 TRAILING: 3 HEADCROP: 10 SLIDINGWINDOW: 4:15 MINLEN: 50. Trimmed reads of all replicates per genotype were pooled and aligned with Bowtie 2[67] to the predicted transcriptome of the reference Morex V1 genome.[61] Output *.sam files were sorted, indexed and converted to *.bam format with SAMtools v1.3.1[68] and read duplicates were marked with the MarkDuplicates tool of Picard v1.141 (http://broadinstitute.github.io/picard). A dictionary and a *.fai index were generated from the reference transcriptome with SAMtools and Picard. Gene variants were called with the HaplotypeCaller tool of GATK v3.5-0[69] and the options SplitNCigarReads and InDel realignment (RealignerTargetCreator and IndelRealigner). This produced a *.g.vcf file including variant information for all transcriptome positions. We also obtained from NCBI's SRA repository, raw RNAseq data of six barley cultivars: Barke (ERR150449), Betzes (ERR150450), Optic (ERR150454), Quench (ERR150455), Sergeant (ERR150456) and Tocada (ERR150457). Moreover, Wilma van Esse and Maria von Korff kindly provided *.bam files of unpublished RNA seq data of cultivars Barke, Bonus, Donaria, Foma, Kindred, Mesa, Montcalm and Scarlett. All these additional datasets were subjected to the procedures outlined above to produce variant *.g.vcf files for each genotype. These files were combined in a single *.vcf with the GenotypeGVCFs option of GATK. This was then converted to a tab-delimited file with vcf-query of VCFtools v0.1.13.[70]

To identify variants unique to *msg38*, the variant file was processed further with R. We excluded the following: a) all variants that appeared 'heterozygous' in *msg38* or that had <3 read depth or <30 GATK quality score; b) all *msg38* variants that were present in any other genotype; c) all variants that showed heterozygosity in any genotype. This filtering left only one polymorphism unique to *msg38* in chromosome 3: the deletion of cytosine 261 in the predicted coding sequence of HORVU.MOREX.r2.3HG0205730 (Morex V2

Please cite this article in press as: Amanda et al., Auxin boosts energy generation pathways to fuel pollen maturation in barley, Current Biology (2022), https://doi.org/10.1016/j.cub.2022.02.073

reference genome assembly),[62] which encodes *HvYUC4*. The deletion shifts the reading frame after codon 88 (out of 355), and shortens it to 237 codons. Sanger sequencing confirmed that this variant is only present in the *msg38* mutant and not in cultivars Ingrid and Bowman. The approximate location of the pericentromeric regions in Figure 3B were estimated according to.[79]

Phylogenetic analysis

YUCCA protein sequences were obtained from EnsemblPlants (http://plants.ensembl.org) using its pre-generated gene trees as guide. Sequences were then manually curated with data from species-specific repositories (e.g. TAIR, maizegdb.org, etc.) and the Gene database at NCBI. Data S1B contains sequence identifiers and curation notes and Data S2 includes all FASTA protein sequences, which were aligned in MEGA-X v10.1.7[71] with the MUSCLE algorithm.[80] The less conserved regions at the N- and C-termini were removed from the alignment, which was exported in NEXUS format to generate a phylogenetic tree with MrBayes v3.2.7,[72] using a Bayesian Inference mixed amino acid model, the Markov Chain Monte Carlo (MCMC) algorithm and 800.000 generations with the standard deviation of split frequencies below 0.01. The tree was visualized with FigTree v1.4.4 (http://tree.bio.ed.ac.uk/software/figtree/), with a *Physcomitrella patens* YUCCA as root, and posterior probabilities added to the nodes.

Agrobacterium-mediated stable plant transformation

Immature embryos of Golden Promise Fast were cultured on Barley Callus Induction Medium containing 5 mg/L dicamba as described.[81] The generated callus tissue was then exposed to *Agrobacterium* strains carrying the plasmids of interest as reported[82] and cultured for 48 hours between filter papers moistened with Barley Co-Cultivation Medium.[82] Callus selection and plant regeneration were as described.[82]

Gene editing

Two sgRNAs targeting *MSG38* were designed with the E-CRISP tool (http://www.e-crisp.org/E-CRISP/, sgRNA1: GGAGGCATCGCA CGTACAAC and sgRNA2 GTCGTCAGCGCCGAATTCAA). Two other sgRNAs targeting *HvYUC2* (HORVU.MOREX.r2.3HG0238160) were later designed with the Cas-Designer tool (http://www.rgenome.net/cas-designer/, sgRNA1: GATCACTGGAGTGAAAGTGA and sgRNA2 GGTTCCTGGTCCTATTATCG). sgRNA specificity was verified with blastn searches on the barley genome. Tom Lawrenson and Wendy Harwood kindly provided the We used published Golden Gate vectors to deliver and express the CRISPR-Cas9-sgRNA system in barley,[64] except that two sgRNAs were expressed from a single plasmid as described for *Brassica oleracea*.[64] (see key resources table for vector list.) The transgene-segregating progeny of Golden Promise Fast plants stably transformed with the CRISPR-Cas9-sgRNA plasmid, was screened for transgene absence with a quick hygromycin resistance test on a piece of cotyledon tissue. Transgene absence was independently confirmed by PCR in hygromycin-susceptible individuals with primers 81unil and 82unil (Data S1N). These individuals were then screened for heritable mutations by PCR and Sanger sequencing.

Auxin metabolite profiling

For each biological replicate, the following stages of Bowman and *msg38* samples were collected in 1.5-ml tubes: W8 (two inflorescences), W8.25–W8.5 (stamens from 17–30 florets), W8.75–W9 and W9.25–W9.35 (stamens from 13–17 florets). Four biological replicates per stage per genotype were harvested. The fresh weight of each replicate was recorded before freezing in liquid nitrogen and storing at -80°C. The extraction, purification and LC-MS analysis of endogenous IAA, its precursors and metabolites were carried out as described.[83] Aapproximately 15 mg of frozen material per sample were homogenized using a bead mill (27 hz, 10 min, 4°C; MixerMill, Retsch GmbH, Haan, Germany) and extracted in 1 ml of 50 mM sodium phosphate buffer containing 1% sodium diethyldithiocarbamate and the mixture of $^{13}C_6$- or deuterium-labelled internal standards. After centrifugation (14000 rpm, 15 min, 4°C), the supernatant was divided in two aliquots. The first aliquot was derivatized by cysteamine (0.25 M; pH 8; 1h; room temperature; Sigma-Aldrich). The second aliquot was immediately processed further as follows: The pH of the extract was adjusted to 2.5 with 1 M HCl and applied on a preconditioned solid-phase extraction column Oasis HLB (30 mg 1 cc, Waters Inc., Milford, MA, USA). After sample application, the column was rinsed with 2 ml 5% methanol. Compounds of interest were then eluted with 2 ml 80% methanol. The derivatized fraction was purified alike. Mass spectrometry analysis and quantification were performed by an LC-MS/MS system comprising a 1290 Infinity Binary LC System coupled to a 6490 Triple Quad LC/MS System with Jet Stream and Dual Ion Funnel technologies (Agilent Technologies, Santa Clara, CA, USA).

RNA Extraction and qRT-PCR

For stage W8, we collected reproductive organs (stamens + pistil from ~40–50 florets) and for all other stages, we sampled only stamens from 7–13 florets. Tissue was collected in 1.5-ml tubes containing a small metal bead, and immediately frozen in liquid nitrogen. Samples were grounded with a TissueLyser II (Qiagen) whose tube holders were pre-frozen at -80C for 10 minutes, then pre-soaked in liquid nitrogen, to guarantee grinding under freezing temperatures. Total RNA was extracted as described,[84] except that 3 units of Promega's DNAse were used. RNA was quantified with a Qubit assay (ThermoFisher Scientific) and all samples were diluted to a 200 ng/μl concentration. cDNAs were synthesized in a 96-well PCR plate with 500 ng total RNA and M-MLV Reverse Transcriptase RNAse H(-) (Promega), scaling down the recommended reaction volume to 10 μl. cDNAs were diluted to 200 μl with water and 2.5 μl were used for qRT-PCR with GoTaq polymerase (Promega) and 0.5X SYBR Green I (ThermoFisher Scientific) in 384-well plates and a LightCycler® 480 II with software v1.5.1.62 (Roche). A putative ADP-ribosylation factor gene (*HvADP*, HORVU.MOREX.r2.3HG0246760) was used for normalization. The data was analyzed with LinRegPCR 2020.0[73] and expression

Please cite this article in press as: Amanda et al., Auxin boosts energy generation pathways to fuel pollen maturation in barley, Current Biology (2022), https://doi.org/10.1016/j.cub.2022.02.073

values calculated in Microsoft Excel 2019: after normalization, the mean expression of each gene at W9.25 was set to 1 and all other samples were calibrated accordingly.

RNA *in situ* hybridization

To generate antisense and sense probe templates, a 450-bp *MSG38* fragment was amplified from Bowman stamen cDNA by PCR with two separate primer pairs that added a T7 promoter (P374+377 for antisense probe and P375+376 for sense probe, Table S17; Data S1N). Purified templates were used to synthesize RNA probes with T7 RNA polymerase and DIG RNA Labeling Mix (Roche). Tissue processing and RNA hybridization were performed mostly as described[85,86] with some modifications. Bowman florets were collected and fixed in 1x Phosphate-buffered saline (PBS, pH 7.4) containing 50% ethanol, 3.7% paraformaldehyde, 2.5% glutaraldehyde, 5% glacial acetic acid, 0.1% Triton X-100 and 0.1% Tween-20. After 1 h of vacuum infiltration, fixation proceeded overnight at 4°C. Samples were dehydrated through an ethanol series and step-wise infiltrated with Histoclear and paraffin. We prepared 10-μm sections of paraffin-embedded tissue with a rotary microtome (RM2065, Leica Microsystems) and placed them on coated glass slides (SuperFrost™ Ultra Plus, Thermo Scientific). Sections were dewaxed with Histoclear and rehydrated in an ethanol series, digested with 0.125 mg/ml Pronase (Roche – Sigma Aldrich) in 50 mM Tris pH 7.5 and 5 mM EDTA, treated with 0.2% glycine to stop the protease, re-fixed in 3.7% formaldehyde, acetylated with 1% acetic anhydride in 0.1M triethanolamine, pH 8.0), rinsed with 1x PBS and dehydrated through an ethanol series. For one pair of slides, 1 out of 50 μl of synthesized RNA probe was diluted in 40 μl of 50% formamide and denatured at 80°C for 2 min. This was added to 160 μl of 80°C-pre-warmed hybridization solution (1.25X in situ salts [0.375M NaCl, 12.5 mM Tris buffer pH 8.0, 12.5 mM Sodium phosphate buffer pH 6.8, 6.25 mM EDTA], 50% deionized formamide, 12.5% dextran sulfate, 1.25X Denhardt's solution [Carl Roth], 0.125 mg/ml yeast tRNA [Roche – Sigma Aldrich]). The hybridization mix was pipetted on one section slide, which was then 'sandwiched' with a second section slide. Slides were elevated in a plastic box containing paper towels saturated with 50% formamide to maintain humidity. Hybridization proceeded overnight at 55°C. Slide sandwiches were carefully separated by dipping in wash solution (0.2x SSC: 60 mM NaCl, 6 mM sodium citrate) and washed twice at 55°C for 30–60 min. Slides were treated with 20 ug/ml RNase A in 1x NTE (0.5 M NaCl, 10 mM Tris-HCl pH 7.5, 1 mM EDTA) at 37°C, rinsed twice with 1x NTE at the same temperature and washed again with 0.2x SSC at 55° C for 1 h. Next, the detection of probe hybridization was carried out at room temperature. Slides were rinsed in 1x TBS (0.4M NaCl, 0.1 M Tris-HCl pH 7.5) and then blocked successively with 0.5% Blocking Reagent (Roche – Sigma Aldrich) in 0.15 M NaCl, 0.1 M Tris-HCl pH 7.5 (45 min) and with buffer A (1% BSA in 0.15 M NaCl, 0.3%, 0.1 M Tris-HCl pH 7.5, Triton X-100, 45 min). Anti-Digoxigenin-AP, Fab fragments (Roche – Sigma Aldrich) were diluted 1:500 in buffer A and added to pairs of slides, which were sandwiched as before and incubated 1 h. After draining the antibody solution with Kimwipe paper, sandwiched slides were separated and washed 4 times in buffer A (20 min each). Colorimetric detection used as substrates 3.5 μl each of NBT and BCIP ready solutions (Roche – Sigma Aldrich) per 1 ml of detection buffer (0.1 M Tris-HCl pH 9.6, 0.1 M NaCl, 50 mM $MgCl_2$). Slides were sandwiched and elevated in box chambers humidified with water-saturated paper towels. Detection proceeded for 24 to 48 h in the dark until signal was visible. Slides were dipped in water to stop the reaction, dehydrated through an ethanol series and mounted with Eukitt® (Sigma-Aldrich) for imaging.

MSG38pro-MSG38-Citrine reporter lines

The gene body of *MSG38* and its 5,898-bp upstream region were obtained by PCR amplification on genomic DNA of the cultivar Morex (primers 401 and 402; Data S1N). The fragment was fused in frame with the gene encoding Citrine Fluorescent Protein via Gateway cloning to create pMP155. The destination vector was pMP154, a modification of pEDO097pFR24GW,[87] where the *in planta* selection cassette was replaced with a hygromycin gene driven by a 2x 35S promoter. However, *Agrobacterium* strains carrying pMP155 did not grow well. Therefore, the plasmid was digested with KpnI to remove 2,906 bp from the 5′ end of the upstream region. The plasmid was then re-circularized by ligation to generate pMP157, carrying a shorter upstream region (3,027 bp) in front of the *MSG38* gene body. Twenty-five T0 plants from 7 independent transformation events in Golden Promise Fast were obtained. Transgene expression was preliminarily evaluated in mature anthers of 22 of these plants and a positive fluorescent signal was found in 18 plants, always in pollen grains only. T1 progenies from 5 independent events were grown and the expression pattern in pollen was confirmed. Four independent lines were propagated and analyzed further. Moreover, they were crossed to *msg38-2* mutants. F2 and F3 progenies were selected by hygromycin resistance, *msg38-2* genotyping and Citrine fluorescence segregation in pollen grains to identify *msg38-2* homozygous mutants that were homo- or hemizygous for the transgene. To specifically amplify the endogenous *MSG38* gene in the transgenic background, primer 649 (specific to Golden Promise and not Morex) was used in combination with primer 165 (Data S1A) to genotype *msg38-2*.

For imaging, stamens were counterstained with 100 μg/ml propidium iodide for 30 mins, mounted in perfluorperhydrophenanthren, and visualized with the SP8 laser confocal scanning microscope (Leica Microsystems). For Citrine Fluorescent Protein, we used the 514-nm laser beam line and HyD detector (emission 520 – 537 nm) and for propidium iodide, the 561-nm laser beam line and HyD detector (emission 613nm - 629 nm). Z-stack images were 3D-reconstructed with Leica Application Suite X v3.5.7, with these settings: opacity=30, Min=5, Max=100, gamma=1 for propidium iodide images and opacity=30, Min=5, Max=80, gamma=0.7 for citrine fluorescent protein images.

Transcriptome analysis

The experimental set-up of the transcriptome analysis is described in the section "*MSG38* gene identification". We used the default settings of the mapping-based mode in Salmon v1.4[74] for RNAseq transcript quantification. This required to create first

Please cite this article in press as: Amanda et al., Auxin boosts energy generation pathways to fuel pollen maturation in barley, Current Biology (2022), https://doi.org/10.1016/j.cub.2022.02.073

a decoy-aware index of the predicted high confidence transcriptome in the reference Morex V2 genome,[62] with the entire genome as decoy sequence. We performed the following analyses with R. All supplementary tables with transcript data show the raw counts for each replicate. We retained only transcripts with >1 count per million (cpm) in all replicates, resulting in an "expressed" set of 19,240 genes (Data S1D). The data was normalized with the TMM method in *edgeR*.[88] Grouping of all biological replicates according to all expressed genes was assessed with principal component analysis and with Euclidean distances plotted with *pheatmap*. This identified two *msg38* replicates (W9.25 R3 and W9.35 R2) as outliers (Figures 5A and 5B), which were excluded from further analyses. We used *limma*[89] to identify differentially expressed genes (DEGs) between *msg38* and Bowman at each stage (W9.25 or W9.35) with a linear model fit on $\log_2$-transformed cpm values and *P* adjustment for false discovery rate (FDR). This produced 3,153 DEGs with a |fold change (FC)| $\geq$ 1.5 and FDR-adjusted $P \leq 0.05$. Hierarchical clustering on DEGs was performed with Pearson correlation coefficients as distance metric, and was drawn as a heatmap with the function annHeatmap2 of Heatplus. We obtained a recently reported *de novo* GO term annotation of the Morex V2 high confidence transcriptome from J. Zhong.[90] Then, we performed Gene Ontology (GO) enrichment analysis in each of the DEG hierarchical clusters with the weigh01 algorithm of the package *TopGO*.[91]

We independently confirmed enrichment by manual or semi-automatic curation of genes encoding specific families or functions. For auxin-responsive genes (Data S1G), the corresponding Arabidopsis proteins from TAIR were used to blastp the Morex V2 proteome; conversely, barley genes annotated as auxin-related in Morex V2[62] were used to blastp the Arabidopsis proteome. In this way, we eliminated spurious annotations or identified previously unannotated genes. A similar procedure was applied to genes encoding sugar transporters (Data S1H), and starch synthesis and degradation enzymes (Data S1I). In this case, the Arabidopsis genes were obtained from Hedhly et al.[92] We believe that we have identified all existing Morex V2 genes in these categories. Lists of barley and rice energy production genes (Data S1I) were downloaded from PlantCyc (https://plantcyc.org/); the barley list was compared to the rice list for completion, based on the orthologous gene groups (orthogroups) reported by J. Zhong.[90] Due to the large size of this list, curation for spurious sequences was done only for genes expressed in our transcriptome; thus, the list of energy production genes may not be exhaustive. Finally, predicted or characterized rice transporter genes obtained from three databases [ARAMEMNON,[93] TransportDB[94] and Rice Transporter Database] were used to identify the corresponding barley genes using J. Zhong's orthogroups. This large list was not curated further. ARAMEMNON was also used to identify rice members of transporter families linked to pollen hydration and tube growth, as summarized by Michard et al.[95] and the barley orthologs were found in J. Zhong's orthogroups (Data S1M).

Prediction of auxin response factor (ARF) binding sites with a machine learning model

We used a machine learning model developed from the DNA binding preference of maize ZmARF35, determined with DNA affinity purification sequencing [DAP-seq[96]]. We fitted a bag-of-k-mers (bok) model for ZmARF35 based on the DAP-seq enriched peaks from maize. The bok machine learning model was generated as described previously.[75,97] In brief, the set of ZmARF35 enriched peaks and its negative control peaks (enriched by HALO-GST tag) were collected from ZmARF35 DAP-seq dataset[96] and randomly divided between training (80%) and testing (20%). We fitted the ZmARF35 bok model from a regularized logistic regression with *k* value equal to 7 bp. The logistic regression used for bok model corresponds to the implementation of the python library scikit-learn (version 0.19.0). The skill of the model is represented in Figure 6D. To predict the potential ZmARF35 binding profile in the Morex V2 barley reference genome, we implemented the scored k-mer vocabularies derived from the trained ZmARF35 model to calculate the predicted probability of ZmARF35 binding a barley fragment of interest. A fragment was considered bound with a predicted probability > 0.85.[97] We extracted the 2-kb upstream sequence from the ATG of all genes expressed in our transcriptome and then fragmented each sequence with a window size of 53 bp. The resulting 53-bp and residual (<53-bp) fragments were evaluated with the ZmARF35 bok model. The predicted binding probabilities and fragment positions were plotted with *pheatmap* in R.

Metabolite profiling and starch measurements

W9.35 stamens from 24 to 31 florets from two inflorescences were dissected with fine forceps and harvested as one biological replicate into 1.5 ml tubes on liquid nitrogen. In total, 5 biological replicates per genotype were analyzed. Metabolite profiling was carried out by gas chromatography (GC)–mass spectrometry (ChromaTOF software v1.00, Pegasus driver 1.61; LECO) as described previously.[98] The chromatograms and mass spectra were evaluated using Xcalibur ™ software (Thermo Scientific). Metabolite identification was manually checked by the mass spectral and retention index collection of the Golm Metabolome Database.[99] Peak heights of the mass fragments were normalized on the basis of the fresh weight of the sample and the added amount of an internal standard (ribitol). Relative levels of each metabolite per sample (Data S1K) were obtained as the ratio between each replicate and the mean of all five Bowman replicates.

Starch levels in the same barley stamen samples were determined with an enzyme-based glucose assay in the GC extraction pellet, essentially as described.[100] Briefly, the pellet was resuspended in 1 ml of deionized water and divided in two aliquots, both of which were boiled at 95°C in a water bath for 20 min. After cooling and a spin at 20000 *g* for 1 min, the water was discarded. We added 50 μl of starch digestion mix (200 mM sodium acetate, 6.3 U/ml amyloglucosidase, 50 U/ml α-amylase, freshly prepared) to the first aliquot for digestion at 37°C for 4 hr. Afterwards, we added 100 μl of glucose assay mix (100 mM 2-(4-[2-hydroxyethyl]-1-piperazinyl)-ethanesulfonic acid-KOH (HEPES-KOH), pH 7.5, 2 mM $MgCl_2$, 20μl 10 mM ATP, 20μl 10 mM NAD^+, 0.3μl 1500 U/ml hexokinase) to both digested and undigested samples and brought them to a final volume of 200 μl in a 96-well flat-bottom microtiter

Please cite this article in press as: Amanda et al., Auxin boosts energy generation pathways to fuel pollen maturation in barley, Current Biology (2022), https://doi.org/10.1016/j.cub.2022.02.073

plate. Meanwhile, we obtained an absorbance plot of glucose standards at 340 nm to determine the linear range and calculate the slope of the standard curve. Baseline absorbance of samples at 340 nm was recorded. After adding 0.45 U of Glucose 6-phosphate dehydrogenase (G6PDH), absorbance at 340 nm was recorded again as ODG6PDH. The starch content was calculated as (ODG6PDH of digested samples−ODG6PDH of undigested samples) − (ODbaseline of digested samples−ODbaseline of undigested samples).

QUANTIFICATION AND STATISTICAL ANALYSIS

Statistical tests used and the exact value of n are found in the figure legends. The description of n for each experiment/analysis is explained in the figure legends and/or the corresponding method details above. Statistical differences between means of Bowman and *msg38* data were determined in Microsoft Excel 2019 with one-tailed Student's t-tests after evaluating homogeneity of variances with *F*-tests, or, where indicated, with one-way ANOVA. The R software environment v4.0.4 in RStudio v1.4.1106 was used for statistical analysis, data processing and plot drawing. The heatmaps in Figures 6A and 6E were created with *heatmap.2* of the package *gplots*. Unless otherwise indicated, all other plots were drawn with the package *ggplot2*. Two outlier replicates in the transcriptome analysis were excluded following principal component analysis and Euclidean sample distance analysis (see "transcriptome analysis" above; Figures 5A and 5B).